E4F1 is essential for epidermal stem cell maintenance and skin homeostasis

Matthieu Lacroix[1, 3, 4, 10, &], Julie Caramel[1, 3, 4, &], Perrine Goguet-Rubio[2, 4], Laetitia Linares[2, 4], Soline Estrach[5], Elodie Hatchi[1, 3, 4], Geneviève Rodier[1, 3, 4], Gwendaline Lledo[2, 4], Carine de Bettignies[1, 2], Amélie Thépot[6], Céline Deraison[8], Karim Chébli[1, 3, 4], Alain Hovnanian[8,9], Pierre Hainaut[6], Pierre Dubus[7], Claude Sardet[1, 3, 4, *] and Laurent Le Cam[1, 2, 3, 4, *].

[1] Institut de Génétique Moléculaire de Montpellier UMR5535 CNRS, Montpellier 34293, France.

[2] Institut de Recherche en Cancérologie de Montpellier, INSERM U896, Montpellier 34298, France.

[3] Université Montpellier 2, Montpellier 34095, cedex 5, France.

[4] Université Montpellier 1, Montpellier 34967, cedex 2, France.

[5] INSERM U.634, Faculté de Medecine, Nice, 06107, France.

[6] IARC, Lyon, 69008, France.

[7] INSERM 33076, France.

[8] INSERM, U563, Toulouse F-31300, France.

[9] current address: CHU Necker-Enfants malades, Département de Génétique, 75015 Paris, France.

[10] current address: INSERM, U563, Toulouse F-31300, France.

* Corresponding authors: claude.sardet@igmm.cnrs.fr (C.S.) and laurent.lecam@inserm.fr (L.L.C.)

[&] equal contribution

Running Title: Role of E4F1 in skin homeostasis

Key words: E4F1, p53, knock-out, epidermal stem cells, skin

Abstract

Growing evidences suggest that the multifunctional protein E4F1 is involved in signalling pathways that play essential roles during normal development and tumorigenesis. Here, we have generated *E4F1* conditional knock-out mice to address E4F1 functions *in vivo* in newborn and adult skin. *E4F1* inactivation in the entire skin or in the basal compartment of the epidermis induces skin homeostasis defects, as evidenced by transient hyperplasia in the interfollicular epithelium and alteration of keratinocyte differentiation, followed by loss of cellularity in the epidermis and severe skin ulcerations. *E4F1* depletion alters Epidermal Stem Cells (ESC) clonogenic activity *ex vivo* and ends in exhaustion of the ESC pool *in vivo*, indicating that the lesions observed in the *E4F1* mutant skin result, at least partly, from cell autonomous alterations in ESC maintenance. Clonogenic potential of *E4F1 KO* ESC is rescued by Bmi1 over-expression or by Ink4a/Arf or p53 depletion. Skin phenotype of *E4F1* KO mice is also delayed in animals with *Ink4a/Arf* and *E4F1* compound gene deficiencies. Our data identify a novel regulatory axis essential for ESC-dependent skin homeostasis implicating E4F1 and the Bmi1-Arf-p53 pathway.

Abbreviations:

ESC, Epidermal Stem Cells; HF, Hair Follicle; 4OHT, 4-Hydroxy Tamoxifen; IFE, Interfollicular Epithelium; K5, K6, K10, K14 and K15, Keratin-5, 6, 10, 14 and 15 respectively; KO, Knock-Out; LRC, Label Retaining Cells; *RERT* , *Cre-ER*^{T2} knock-in mice; TAC, Transit Amplifying Compartment.

/body **Introduction:**

E4F1 is an ubiquitously expressed transcription factor of the Gli-Kruppel family that was identified as a cellular target of the adenoviral oncoprotein E1A (1). While several cellular targets of E1A (E2F/pRB, CBP/p300, PCAF, CtBP, ATF/Creb etc…) have been extensively studied and recognized as central regulators of cell proliferation and survival, E4F1 biological functions remained poorly investigated. E4F1 is a multifunctional protein with transcriptional and atypical ubiquitin E3-ligase activities. E4F1-mediated ubiquitylation of p53 does not lead to proteasomal degradation but modulates p53 transcriptional activities involved in alternative cell fates: growth arrest or apoptosis (2). The notion that E4F1 plays an important role in the p53 pathway is reinforced by other reports showing that E4F1 not only directly interacts with p53 itself (2, 3) but also with regulators/effectors of this pathway, including $p14^{ARF}$ (4), the polycomb member Bmi1 (5), and the p53 target gene FHL2 (6). Nevertheless, E4F1 functions most likely extend beyond the regulation of p53. Thus, physical interactions between E4F1 and components of other oncogenic pathways have been reported, including RASSF1A (7), pRB (8), HMGA2 (9) and Smad4 (10).

Using a gene targeting approach in mouse, we previously showed that *E4F1* constitutive inactivation results in embryonic lethality around the time of implantation. *E4F1 KO* blastocysts in culture exhibit mitotic defects including lagging chromosomes, chronic activation of the mitotic checkpoint, and massive cell death (11). More recently, shRNA-mediated partial depletion of E4F1 was also shown to rescue hematopoietic stem cell (HSC) exhaustion in mouse resulting from inactivation of the polycomb member *Bmi1* (5), suggesting an important role for E4F1 in HSC homeostasis.

To date, little information is currently available regarding the *in vivo* functions of E4F1 in adult tissues. Here, we generated several mouse strains to explore the roles of E4F1 in skin homeostasis.

Constant renewal of the Interfollicular Epithelium (IFE) and of Hair Follicles (HF) relies on the recruitment of epidermal stem cells (ESC) located in the basal layer of the IFE and in the bulge region of HF, respectively. ESC fuel the highly proliferative transit amplifying compartments (TAC) in the basal layer of the IFE and in the bulb of the HF. TAC cells then embark on differentiation programs to generate the spinous, granular and cornified layers in the IFE or the different lineages of the mature HF (12-14). Several essential molecular circuitries that orchestrate epidermal stem cells maintenance have been previously described, including p63-, BMP-, TGF-ß-, Wnt/ß-catenin-, and Notch-initiated signalling cascades (12, 15, 16).

Here, we show that inactivation of *E4F1* in the entire skin or in the basal compartment of the epidermis results in severe epidermal defects both in neonates and in adult mice, revealing a yet unidentified regulatory axis essential for ESC-dependent skin homeostasis implicating E4F1 and the Bmi1-Ink4a/Arf-p53 pathway.

Results:

Inactivation of *E4F1* induces transient hyperplasia in the epidermis followed by permanent loss of epidermal cells and severe skin ulcerations.

We first investigated E4F1 expression pattern in epidermis. Immunohistochemical analyses of murine and human skin sections showed nuclear expression of E4F1 in the basal and suprabasal layers of the interfollicular epithelium (IFE), as well as in the bulb and bulge regions of the hair follicle (HF) (Fig. 1A).

To analyse the role of E4F1 in skin homeostasis, we generated two mouse models with homozygote deletion of the *E4F1* gene in the entire skin or in the epidermis only, using conditional (*Cre-ER*^{T2}) and tissue specific (*K5-Cre*) *Cre/Lox-P* systems, respectively. In short, we first generated *E4F1*$^{-/flox}$ mice harboring *E4F1* conditional knock-out allele (Fig. S1) and inter-crossed them with *Cre-ER*$^{T2\ KI/KI}$ mice (*RERT*) which express tamoxifen-inducible Cre recombinase-ER^{T2} fusion protein under the control of the ubiquitously active *RNA polII* promoter, i.e. in all tissues (17). As expected, topical applications of 4-hydroxy-tamoxifen (4OHT) on the tail skin or on a shaved area of the back skin of adult *E4F1*$^{-/flox}$; *RERT* animals, resulted in efficient Cre-mediated recombination of the *E4F1* locus in the skin, as monitored on genomic DNA, mRNA and protein samples prepared from the treated area (Fig. S1).

Between 1 and 2 weeks after 4OHT-administration, E4F1-depleted back skin thickened, became wrinkled and ruffled. Those early lesions evolved 1 to 2 weeks later into severe skin ulcerative lesions (Fig. 1B). Strikingly, *E4F1* inactivation in unshaved skin tail of *E4F1*$^{-/flox}$*; RERT* animals resulted in complete alopecia 6 weeks after 4OHT applications (Fig. 1C). Histological analyses revealed that skin thickening was the result of a massive hyperplasia of the epidermis with increased cellularity in the IFE and the infundibulum (Fig. 1D). Consistent with the observed hyperplasia, an abnormal proportion of epidermal cells

were proliferating in *E4F1* KO skin, as indicated by increased immunostaining of skin sections for the proliferation marker Ki67 (Fig. 1D), and anti-BrdU staining performed on skin sections harvested shortly after injection of animals with BrdU (Fig. S2). This phenotype was skin autonomous since similar hyperplasia was recapitulated upon engraftment of *E4F1*$^{-/flox}$*; RERT* p1 neonatal back skin onto nude mice (Fig. S3). At later time points (3 to 4 weeks after 4OHT administration), the initial hyperplasia of *E4F1 KO; RERT* skin was followed by broad disorganisation of the IFE and massive hyperkeratosis associated with partial or complete loss of cellularity in the IFE (Fig. 1D).

To further show that the observed phenotypes resulted from epidermis specific defects, we crossed *E4F1*$^{-/flox}$ mice with *Keratin 5-Cre* (K5-Cre) transgenic mice expressing Cre in the epidermal basal cell layer, from E15.5 onwards (18). *E4F1*$^{-/flox}$; *K5-Cre* neonates exhibited efficient *E4F1* gene inactivation in the epidermis as shown by immunohistochemical staining and western-blot analyses with anti-E4F1 antibodies (Fig. 1E and S1). 3 to 4 days after birth, these animals exhibited epidermal hyperplasia, and died with acute symptoms of dehydration (Fig. 1F). As in *E4F*$^{-/flox}$*; RERT* animals, this hyperplasia was associated with hyperproliferation of epidermal cells, as shown by increased Ki67 staining (Fig. 1G). Consistent with increased proliferation, *E4F1* KO epidermis also exhibited higher mitotic index, as illustrated by increased number of phospho histone H3 (Ser10, PHH3) positive basal cells (Fig. S5). Of note, we previously showed that *E4F1* KO blastocysts also exhibited PHH3-positive cells (11), but in this case, cells were blocked in mitosis with abnormal mitotic figures. We did not observe abnormal mitotic figures in *E4F1* KO epidermal basal cells, indicating that the increased mitotic index likely reflects over-proliferation of basal cells, rather than mitotic progression defects.

In order to bypass neonatal lethality of *E4F1 KO; K5-Cre* animals and investigate later phenotypes, we engrafted *E4F*$^{-/flox}$*; K5-Cre* or control skins onto nude mice. 2 weeks after

engraftment, *E4F1 KO; K5-Cre* skins failed to regenerate a normal epidermis. Similarly to the late phenotype of *E4F*$^{-/flox}$*; RERT* animals, *E4F1 KO, K5-Cre* engrafted skins exhibited marked hypocellularity in the epidermis, hyperkeratosis and severe ulcerative lesions (Fig. 1H). Of note, hair follicles were also lacking in *E4F1 KO, K5-Cre* engrafted skins. Collectively, our data indicate that *E4F1* inactivation results in transient hyperplasia but ultimately leads to permanent loss of epidermal cells in the IFE and HFs.

E4F1* inactivation results in expansion of the basal cells compartment of the epidermis and in abnormal keratinocyte differentiation *in vivo.

We next assessed which epidermal cell populations were present in these hyperplasic lesions. In both 4OHT-treated *E4F1*$^{-/flox}$*; RERT* and *E4F1*$^{-/flox}$*; K5-Cre* epidermis, cells of the hyperplasic IFE stained positive for the basal cell-specific keratin-14, integrin-α6, markers (Fig. 2A and S4). Expression of these markers extended to upper cellular layers, in contrast to normal IFE of control animals where their expression was restricted to the basal cell layer. In addition, *E4F1*-floxed IFE massively expressed keratin-6 (Fig. 2B and S4), which expression is normally restricted to sweat glands and HF in normal skin but can be expressed in the IFE undergoing abnormal proliferation or wound healing (19). Collectively, these analyses indicated that *E4F1* inactivation in the IFE first resulted in massive expansion of keratinocytes with basal/TAC properties.

In addition to this massive expansion of basal cells, we noticed the absence of the suprabasal and granular layers as illustrated by the lack of expression of early (keratins 1 and 10), as well as late differentiation markers (involucrin, loricrin, filaggrin) in *E4F1 KO* epidermis in both *E4F1*^{flox}*; K5-Cre* and *E4F1*^{flox}*; RERT* models (Fig. 2B, S4). No significant cell death was observed among highly proliferative cells of the IFE during the development of hyperplasia, as revealed by immunostaining of skin sections for the presence of activated

caspase 3- or TUNEL-positive cells. Therefore, it is likely that hyperproliferative keratinocytes present in hyperplasic lesions had finally undergone an abnormal differentiation program of stratification, rather than apoptosis, leading to the observed hyperkeratosis. These data indicate that *E4F1* inactivation strongly perturbates both the proliferation and differentiation of epidermal lineages *in vivo* leading to a strong alteration of skin homeostasis.

***E4F1* inactivation induces epidermal stem cell defects.**

We next investigated the mechanisms by which *E4F1* inactivation in the IFE led to a massive but transient expansion of the basal/TAC compartment, followed by its exhaustion. Several scenarios could explain this sequence of events. First this could reflect an increase in the intrinsic capacity of basal/TAC keratinocytes to proliferate. However, this is unlikely, since E4F1 depletion in freshly isolated populations of primary keratinocytes in culture did not recapitulate the massive over-proliferation observed in skin sections, as illustrated by FACScan analyses of BrdU/Propidium Iodide- (PI) or PHH3/PI-labelled keratinocytes isolated from *E4F1*$^{-/flox}$*; RERT* or control p1 neonates (Fig. S5). Similar conclusions were obtained in primary human keratinocytes upon shRNA-mediated depletion of endogenous human *E4F1* (Fig. S5). These observations, together with the withering and transient aspect of the hypertrophy phenotypes led us to investigate an alternative hypothesis involving perturbations of the resident stem cells (ESC). Several aspects of *E4F1* KO phenotypes are reminiscent of skin lesions observed in KO animals exhibiting stem cell defects. Hence, conditional perturbation in the epidermis of several key signalling molecules, including the small GTPase Rac1, Myc, Smad4, NFATC1, leads ESC to exit their normal microenvironment (“niche”) to enter into the TAC where they become transiently proliferating keratinocytes upon exposition to natural pro-mitogenic signals present in this amplification compartment (20-24). This results in transient hyperplasia followed by a

permanent exhaustion of the epidermal stem cell pool and loss of renewal capacity of the epithelium.

To address this scenario, we first performed standard *in vitro* clonogenic assays on feeder layers with total primary keratinocytes isolated from *in vivo* recombined hyperplasic regions of *E4F1*$^{-/flox}$*; RERT* adult mice, as well as from *E4F1*$^{-/flox}$*; K5-Cre* p1 neonates or control littermates. After 10 to 15 days in culture, typical holoclones, corresponding to the long-term clonal outgrowth of epidermal cells with stem cell properties (25, 26) were detected in controls but not in *E4F1* KO conditions in both models (Fig. 3A). Importantly, similar results were recapitulated when *E4F1* inactivation was induced *ex vivo* by adding 4OHT in the culture medium of *E4F1*$^{-/flox}$*; RERT* cells (Fig. 3A), showing that these defects were stem cell autonomous. Similarly, clonogenic assays performed with primary human keratinocytes transduced *ex vivo* with *E4F1* shRNA constructs showed that partial *E4F1* depletion resulted in a 3 fold reduction in the number of holoclones (Fig. 3B).

We next investigated whether *E4F1* inactivation also resulted in exhaustion of the stem cell pool *in vivo* by analysing expression of various ESC markers. FACscan analyses of dissociated epidermis revealed that *E4F1*$^{-/flox}$*; K5-Cre* neonatal epidermis contained fewer ESC co-expressing the CD34 surface marker and high levels of α6-integrin ($CD34^{+}/\alpha6^{high}$) than control epidermis (8% +/- 2 vs 1,5% +/- 1, n=3) (Fig. 3C). Similarly, immunostainings performed on back skin sections or on whole mount of tail epidermis harvested from adult *E4F1*$^{-/flox}$*; RERT* animals 4 to 6 weeks following *E4F1* inactivation, showed loss of expression of the HF bulge markers CD34 and keratin-15 (Fig. 3D and S6).

To confirm these HF ESC defects *in vivo*, we crossed *E4F1*$^{-/flox}$*; RERT* animals with *Keratin15-EGFP* (*K15-GFP*) transgenic mice expressing the GFP reporter under the control of the keratin-15 promoter (27). In 7 to 12-week-old *K15-GFP; E4F1*$^{+/flox}$*; RERT* control animals, GFP expression was restricted to the bulge region of unsynchronized HF. In contrast,

complete loss of GFP-positive cells was observed 4 to 6 weeks after *E4F1* inactivation in *E4F1 KO; RERT* animals, confirming the exhaustion of the HF ESC (Fig. 3E). Finally, we tracked HF bulge/ESC as BrdU Long Term Retaining Cells (LRC) using an *in vivo* labelling protocol that marks self-renewing and multi-potent epidermal cells (26, 28). *E4F1*$^{-/flox}$*; RERT* and *E4F1*$^{+/flox}$*; RERT* neonates were injected with BrdU and after a chase period of three months, the poorly proliferative adult ESC were identified on whole mounts of tail epidermis, as BrdU-positive LRC. 2 to 3 weeks after *E4F1* inactivation the LRC zone extended and an increased numbers of LRCs were co-labeled with Ki67 in *E4F1 KO* HF as compared to control HF (Fig. 3F early and S7), suggesting that *E4F1* inactivation induced HF ESC to transiently proliferate. At later time points (6 weeks after 4OHT), whereas LRCs were still restricted to the bulge of control HF, BrdU staining finally disappeared in the *E4F1* KO HF (Fig. 3F late), supporting the notion that the end result of *E4F1* inactivation was an exhaustion of the ESC pool. Finally, consistent with the role of ESC in regenerating the various epithelial cell types of hairy skin after injury (26), we also observed that wound healing was strongly altered in *E4F1* KO skin (figure S8). Altogether, these data indicate that *E4F1* is essential for ESC maintenance *in vivo* and *ex vivo,* and strongly suggest that the hyperplasia and following loss of cellularity of *E4F1 KO* epidermis, are primarily due to cell autonomous perturbations of the ESC pool that aliments TAC compartments.

Down regulation of the Bmi1-Ink4a/Arf-p53 axis partly rescues ESC-clonogenic potential and skin lesions of *E4F1 KO*.

We next addressed the molecular pathway by which E4F1 could regulate ESC maintenance. E4F1 associates with the polycomb member Bmi1 and the tumor suppressors Arf, p53 and pRb (2-5, 8). Although there are evidences that these factors have independent functions, they define a well established functional cascade with Bmi1 triggering the

repression of the *Ink4a/Arf* locus whose products, $p19^{Arf}$ and $p16^{Ink4a}$, act as potent inhibitors of the p53- and pRb-dependent activities, respectively (29). Several reports suggest that the negative regulation of *Ink4a/Arf* expression may be a central event in stem cell renewal in several tissues (30-33) including epidermis (34). Strikingly, we observed that *E4F1 KO* primary keratinocytes exhibited enhanced *Ink4a* and *Arf* mRNA levels compared to control cells (Fig. 4A), suggesting that the deregulation of the *Ink4a/Arf* locus might be involved in *E4F1 KO* phenotype. Consistent with this hypothesis, clonogenic assays performed with primary keratinocytes isolated from *E4F1*$^{-/flox}$*; RERT; Ink4a/Arf*$^{-/-}$ compound mice showed that *Ink4a/Arf* inactivation partly restored long-term outgrowth of *E4F1 KO* ESC *ex-vivo* (Fig. 4B, C). The number of viable clones growing in this condition was similar to that obtained from control skin.

Importantly, the *in vivo* skin phenotype of *E4F1 KO* mice was also delayed in animals with *Ink4a/Arf* and *E4F1* compound gene deficiencies. Hence, the initial epidermal hyperplasia of 4OHT-treated *E4F1*$^{-/flox}$*; RERT; Ink4a/Arf*$^{-/-}$ animals was almost undetectable at early time points following *E4F1* inactivation (Fig. 4D, early), compared to control littermates with *E4F1* KO only. Nevertheless, at later time points, these animals ended up to develop a moderate hyperplasia and hyperkeratosis (Fig. 4D, late).

To provide further evidence for a role of the Ink4a/Arf–pRb/p53 cascades in *E4F1 KO* phenotype, we next tried to rescue the clonogenic potential of *E4F1 KO* ESC by targeting Bmi1, one of the main upstream regulator of the *Ink4a/Arf* locus. Transduction of keratinocytes by retroviruses expressing Bmi1 rescued long-term outgrowth and clonogenic potential of *E4F1 KO* cells (4OHT-treated *E4F*$^{-/flox}$*; RERT* keratinocytes) (Fig. 5A and 5C).

To assess which *Ink4a/Arf* downstream targets might be involved, clonogenic assays were also performed upon shRNA-mediated (lentiviral vectors) depletion of either murine *RB1* or *p53* in *E4F1 KO* keratinocytes. p53 (Fig. 5B and 5C) but not pRb depletion restored

clonal outgrowth of *E4F1 KO* keratinocytes, highlighting the role of the Bmi-Arf-p53 axis rather than the Bmi-p16-pRb axis in *E4F1 KO* skin phenotypes. Of note, *E4F1 KO* rescued clones that developed upon inactivation of *Ink4a/Arf*, depletion of p53 or overexpression of Bmi1, all remained significantly smaller in size, compared to those growing from control cells (Fig. 4B-C, 5A-B), suggesting that E4F1 might also impinge on other molecular circuitries that orchestrate ESC maintenance.

Altogether, our data provide the first evidence that E4F1 is essential for ESC-dependent skin homeostasis and identify a novel regulatory axis involved in this process implicating Bmi1 and the Arf-p53 pathway.

Discussion

In vivo functions of E4F1 remain poorly documented. Here, we created E4F1 conditional KO mice and reported that *E4F1* inactivation in the epidermis led to neonatal lethality that resulted from skin homeostasis defects. We found that E4F1 depletion in *E4F1 KO; K5-Cre* neonates first led to a rapid thickening of the IFE associated with increased numbers of highly proliferative keratinocytes in the basal cell layers (TAC compartment) of the IFE. Comparable results were obtained upon E4F1 inactivation in adult skin obtained by topical applications of 4OHT on the back skin of $E4F1^{-/flox}$*; RERT* mice. In both *E4F1 KO* models, hyperplasia was transient and followed by a severe disorganization and almost complete loss of viable epithelial cell layers in the IFE and HF. In addition, perturbations of epidermal differentiation were observed in *E4F1* depleted epidermis, in both models.

Strikingly, *E4F1* depletion *in vitro*, in freshly isolated populations of murine or human primary keratinocytes in culture, did not recapitulate the over-proliferation observed in skin sections, ruling out the possibility that the hyperplasia originates from an intrinsic increase in the proliferation capacity of *E4F1* KO TAC keratinocytes. As described for other gene deficiencies in epidermis (20, 22), our data rather suggest that *E4F1 KO* phenotypes resulted from cell autonomous perturbations in resident stem cells. Indeed, *E4F1* depletion *in vivo* or *ex vivo* turned out to dramatically impair the clonogenic potential of both murine and human epidermal cell populations. In addition, a strong reduction in the expression of various ESC markers was observed *in vivo* in *E4F1* KO skins. Finally, BrdU labelling of LRC suggested that *E4F1 KO* HF stem cells first exited their normal location in the bulge region of the HFs to enter in a transient phase of proliferation, before disappearing. As predicted by this stem cell-oriented scenario, exhaustion of the resident stem cell pool in *E4F1* KO skin ultimately led to a complete loss of cellularity in the IFE and alteration of wound healing.

Seeking for the pathway by which E4F1 could regulate ESC maintenance, we found that the clonogenic potential of *E4F1 KO* ESC was restored upon targeting of the Bmi1-Ink4a/Arf-p53 axis but not by pRb depletion, highlighting the role of the Bmi-Arf-p53 axis rather than the Bmi-p16-pRb axis in *E4F1 KO* skin phenotypes. Consistently, E4F1 inactivation correlated with increased Ink4a/ARF expression and our *in vivo* data showed that the development of hyperplasia was delayed and reduced in animals with *Ink4a/Arf* and *E4F1* compound gene deficiencies. It remains unclear how this protein network impinges on ESC homeostasis and ultimately raises the question about the physiological functions of this Bmi1-Ink4a/Arf-p53 axis in ESC. Although poorly documented, it has been suggested that it might play its usual "gate-keeper" function in these cells, notably in response to genotoxic or developmental stresses, as illustrated in mice with dysfunctional telomeres (35, 36) or in *p63 KO* mice (34, 37). As described in other tissues, it is also formally possible that the Bmi1-ARF-p53 protein network plays a role in the normal program of ESC self-renewal and maintenance. Hence, in absence of acute genotoxic stress, inactivation of *p53* or *Ink4a/Arf* has been shown to impact on the self-renewal capacity of hematopoietic multipotent progenitors (38) and neural stem cells (39). Even more intriguing is the recent finding that *p53 KO* favours symmetric divisions and self-renewal capacity of mammary gland progenitor cells (40). The latter observation raises questions about similar roles of p53, and indirectly E4F1, in the epidermis where proper columnar stratification and tissue organization are driven, at least in part, by oriented, asymmetric cell divisions (41, 42).

Our data also highlight the complexity of E4F1 connections with the polycomb family member Bmi1. Indeed, others have shown that shRNA-mediated depletion of E4F1 can rescue premature senescence of *Bmi1* KO hematopoietic stem cells and restore the viability of animals transplanted with those rescued cells, in a *Ink4a/Arf*- and *p53*-independent manner (5). Our data indicate that the genetic links between E4F1 and Bmi1 in stem cell maintenance

are complex and might differ from one tissue to the other since in epidermis, we clearly observed that Bmi1 ectopic overexpression partly rescued stem cell defects of *E4F1 KO* ESC. Of note, we currently do not rule out that E4F1 might also exert yet unidentified additional cellular functions independent from Bmi1 and the Arf-p53 axis. Supporting this notion, we found that targeting the Bmi1-Arf-p53 axis did not fully restore ESC clonal outgrowth and normal skin phenotype. Animals with *Ink4a/Arf* and *E4F1* compound gene deficiencies ended up to develop a moderate hyperplasia and hyperkeratosis at late time points. Likewise, in clonogenic assays, *E4F1 KO* rescued clones that developed upon depletion of p53 or *Ink4a/Arf*, or upon over-expression of Bmi1, all remained significantly smaller in size, compared to those growing from control cells. Therefore, in addition to its connection with the Bmi1-Arf-p53 cascade, one could hypothesize that E4F1 might also impinge on other *hitherto* described molecular circuitries that orchestrate epidermal stem cells maintenance, including TGFß-, Wnt/ß-catenin-, or Notch-initiated signalling cascades (12-14). Interestingly, a physical interaction of E4F1 with Smad4 has recently been shown in BMP-mediated regulation of myogenic differentiation (10). Further studies will be required to evaluate whether this interaction is also implicated in epidermal homeostasis.

In conclusion, the roadblock to developing an *E4F1* conditional KO mouse has been overcome and provides the first evidence, that E4F1, through its connection with the Bmi1 and the Ink4a/Arf-p53 axis, is an important player of stem cells-dependent skin homeostasis. This finding, together with previous reports showing that E4F1 is targeted by several oncoproteins and tumor suppressors, also raise an interesting question about E4F1 potential implication in the development/maintenance of cancer stem cells which presence is suspected in several cutaneous malignancies, including skin carcinoma and malignant melanoma.

Material and Methods:

Ethics Statement

All experiments involving mice were approved by Montpellier's ethic committee for animal warefare.

Generation of *E4F1*$^{-/flox}$ mice and experimental treatment of mice

Generation of the *E4F1*^{flox} allele and of *E4F1*$^{-/flox}$ mice are detailed in supplementary informations (SI). *E4F1*$^{-/flox}$ mice were crossed with *Cre-ER*^{T2} knock-in mice (*RERT*) (17) or *Keratin5-Cre* transgenic mice (18) to obtain *E4F1*$^{-/flox}$; *RERT*$^{KI/KI}$ animals, and *E4F1*$^{-/flox}$; *K5-Cre* animals, respectively. *E4F1*^{flox}*; RERT* mice were also crossed with homozygous *Keratin15-EGFP* transgenic mice (Jackson lab) (27) to generate *E4F1*^{flox}*; RERT*$^{KI/KI}$; *K15-GFP* animals and with *Ink4a/Arf* $^{-/-}$ mice (43) to generate *E4F1*^{flox}*; RERT*$^{KI/KI}$*; Ink4a/Arf* $^{-/-}$ animals. *E4F1* recombination in adult *E4F1*^{flox}*; RERT* skin was induced by topical applications of 4-hydroxy Tamoxifen (4OHT) (Sigma) (2mg dissolved in ethanol per application per day, 4 applications total), on the shaved back skin or the tail. For skin grafting experiments, dorsal skin from *E4F1*^{flox}*; RERT* or *E4F1*^{flox}*; K5-Cre* neonate donors were transplanted onto athymic nude recipient mice (Charles River), as previously described (44). For visualisation of BrdU-label-retaining cells (LRC), ten days old mice were injected with BrdU (50mg/kg of body weight, Sigma) every 12 hours for a total of four injections. To achieve short-term labeling of cells undergoing DNA synthesis *in vivo* (for IHC experiments), BrdU (50mg/kg of body weight) was injected intra-peritoneally, 4 hours prior to euthanasia.

Histochemistry, immunolabelling of skin sections and whole mounts

Immunohistochemistry of skin sections was performed as described in SI with the following primary antibodies: anti -E4F1 (B-21 rabbit polyclonal) generated by our laboratory, -Ki67 (#SP6, Neomarkers), -keratin 6 (#SPM269, Abcam), -keratin10 (#PRB-159P, Covance), -

involucrin (#Sc15230, Santa Cruz), -CD34 (RAM34, BD Pharmingen), and -keratin 15 (#LHK15, Vector Laboratories). Immunohistofluorescence stainings with anti-α6-integrin (#GoH3, BD Biosciences) and anti-keratin 14 (#AF64, Covance) were performed on 10μm cryosections fixed for 10 minutes in 100% acetone. BrdU-positive cells were detected using anti-BrdU antibody (BD Biosciences). Whole mounts of tail epidermis and detection of LRC were prepared as described previously (28) and pictures were generated using a Zeiss 510 confocal microscope and presented as Z-stack projections after deconvolution with Imaris software.

Culture of primary keratinocytes and clonogenic assays

Murine primary keratinocytes were isolated from newborn skin after overnight treatment with dispase (5 mg/mL, Roche) or from adult back skin after trypsin-EDTA overnight treatment, and grown in calcium-free EMEM medium (Biowhittaker, Lonza), containing 10% calcium-free FCS (Sigma) and 10 μg/ml murine EGF (Roche). Cre-mediated recombination of E4F1 flox alleles were achieved by adding 4OHT (1 μM, Sigma) in the culture medium. Human primary keratinocytes were isolated from skin biopsies obtained after medical surgery and cultured in Green medium containing 1,2 mM calcium as previously described (45) and according to Helsinki Declaration. Clonogenic assays were perfomed as described in SI. Colonies were fixed with 4% PFA and stained with 1% Rhodamine B (Sigma). Quantitative analysis of the total number and size of clones was performed with ImageJ.

Retroviral and lentiviral particles productions and infections

Viral particles were produced as described in SI, with the following constructs: pMSCV-Bmi1 (29), pMKO vector encoding either control or anti human *E4F1* shRNAs (sequences available upon request); pLKO1 encoding shRNAs directed against murine RB1 or p53 (Sigma mission shRNA clones, NM_011640.1-625s1c1), or control irrelevant sequence.

Western blotting

Total cell extracts were prepared in 50 mM Tris-HCl, pH 7.4, 100 mM NaCl, 5 mM EDTA, 0,5% NP40, supplemented with protease inhibitors (Complete, Roche). Immunoblots were probed with primary antibodies directed against E4F1 (8), p53 (1C12, Cell signalling), Bmi1 (#F6, Millipore), β-actin (Sigma)

FACScan analyses

Freshly isolated cell suspensions were incubated with FITC-conjugated anti-CD34 (RAM34, BD Biosciences) and PE-Cy5-conjugated anti-α6-integrin primary antibodies for 30 minutes at 4°C. For cell cycle analyses, formalin-fixed cells were incubated with anti-BrdU or anti-phospho-serine 10 histone H3 (6G3 #9706, Cell Signalling) and PI (Sigma) as previously described (2). Cells were analysed on a FACS Calibur (Becton Dickinson) and data were processed with Flowjo software (Treestar).

Acknowledgments

We are grateful to all members of the LLC and CS laboratories for helpful discussions and critical readings of the manuscript, to C. Jacquet, E. Jouffre and P. Cavelier for technical help in mouse handling and histological analyses. We thank the "Clinique de la souris, Strasbourg" for injection of E4F1 flox ES cells into blastocysts. We thank C. Blanpain and M. Van Lohuizen for reagents and advices, as well as, J. Jorcano, A. Ramirez, A. Gandarillas, M. Barbacid and M. Serrano for providing us with *K5-Cre* transgenic, *RERT* knock-in and *ink4a/Arf*$^{-/-}$ mice. Microscopy imaging and histological analyses were performed on the MRI imaging core facility (Montpellier) and RHEM histology (Montpellier) facility, respectively. CS and JC are supported by the Agence Nationale pour la Recherche (ANR blanche), by the AICR foundation, by la Fondation pour la Recherche Médicale (Equipe labellisée 2007) and by institutional supports from CNRS. LLC is supported by the INSERM Avenir Program and the Association pour la Recherche contre le Cancer. ML and EH are supported by fellowships from ARC.

References:

1. Raychaudhuri P, Rooney R, & Nevins JR (1987) Identification of an E1A-inducible cellular factor that interacts with regulatory sequences within the adenovirus E4 promoter. *Embo J* 6(13):4073-4081.
2. Le Cam L*, et al.* (2006) E4F1 is an atypical ubiquitin ligase that modulates p53 effector functions independently of degradation. *Cell.* 127(4):775-788.
3. Sandy P*, et al.* (2000) p53 is involved in the p120E4F-mediated growth arrest. *Oncogene* 19(2):188-199.
4. Rizos H*, et al.* (2003) Association of p14ARF with the p120E4F transcriptional repressor enhances cell cycle inhibition. *J Biol Chem* 278(7):4981-4989.
5. Chagraoui J*, et al.* (2006) E4F1: a novel candidate factor for mediating BMI1 function in primitive hematopoietic cells. *Genes Dev.* 20(15):2110-2120.
6. Paul C*, et al.* (2006) The LIM-only protein FHL2 is a negative regulator of E4F1. *Oncogene.* 25(40):5475-5484. Epub 2006 May 5471.
7. Fenton SL*, et al.* (2004) Identification of the E1A-regulated transcription factor p120 E4F as an interacting partner of the RASSF1A candidate tumor suppressor gene. *Cancer Res* 64(1):102-107.
8. Fajas L*, et al.* (2000) pRB binds to and modulates the transrepressing activity of the E1A-regulated transcription factor p120E4F. *Proc Natl Acad Sci U S A* 97(14):7738-7743.
9. Tessari MA*, et al.* (2003) Transcriptional activation of the cyclin A gene by the architectural transcription factor HMGA2. *Mol Cell Biol* 23(24):9104-9116.
10. Nojima J*, et al.* Dual roles of smad proteins in the conversion from myoblasts to osteoblastic cells by bone morphogenetic proteins. *J Biol Chem* 285(20):15577-15586.
11. Le Cam L, Lacroix M, Ciemerych MA, Sardet C, & Sicinski P (2004) The E4F protein is required for mitotic progression during embryonic cell cycles. *Mol Cell Biol* 24(14):6467-6475.
12. Blanpain C & Fuchs E (2009) Epidermal homeostasis: a balancing act of stem cells in the skin. *Nat Rev Mol Cell Biol* 10(3):207-217.
13. Cotsarelis G (2006) Epithelial stem cells: a folliculocentric view. *J Invest Dermatol* 126(7):1459-1468.
14. Brouard M & Barrandon Y (2003) Controlling skin morphogenesis: hope and despair. *Curr Opin Biotechnol* 14(5):520-525.
15. Dotto GP (2008) Notch tumor suppressor function. *Oncogene* 27(38):5115-5123.
16. Candi E*, et al.* (2008) p63 in epithelial development. *Cell Mol Life Sci.* 65(20):3126-3133.
17. Guerra C*, et al.* (2003) Tumor induction by an endogenous K-ras oncogene is highly dependent on cellular context. *Cancer Cell.* 4(2):111-120.
18. Ramirez A*, et al.* (2004) A keratin K5Cre transgenic line appropriate for tissue-specific or generalized Cre-mediated recombination. *Genesis.* 39(1):52-57.
19. Weiss RA, Eichner R, & Sun TT (1984) Monoclonal antibody analysis of keratin expression in epidermal diseases: a 48- and 56-kdalton keratin as molecular markers for hyperproliferative keratinocytes. *J Cell Biol* 98(4):1397-1406.
20. Benitah SA, Frye M, Glogauer M, & Watt FM (2005) Stem cell depletion through epidermal deletion of Rac1. *Science.* 309(5736):933-935.
21. Horsley V, Aliprantis AO, Polak L, Glimcher LH, & Fuchs E (2008) NFATc1 balances quiescence and proliferation of skin stem cells. *Cell* 132(2):299-310.
22. Yang L, Wang L, & Yang X (2009) Disruption of Smad4 in mouse epidermis leads to

depletion of follicle stem cells. *Mol Biol Cell* 20(3):882-890.
23. Waikel RL, Kawachi Y, Waikel PA, Wang XJ, & Roop DR (2001) Deregulated expression of c-Myc depletes epidermal stem cells. *Nat Genet* 28(2):165-168.
24. Arnold I & Watt FM (2001) c-Myc activation in transgenic mouse epidermis results in mobilization of stem cells and differentiation of their progeny. *Curr Biol* 11(8):558-568.
25. Barrandon Y & Green H (1987) Three clonal types of keratinocyte with different capacities for multiplication. *Proc Natl Acad Sci U S A* 84(8):2302-2306.
26. Blanpain C, Lowry WE, Geoghegan A, Polak L, & Fuchs E (2004) Self-renewal, multipotency, and the existence of two cell populations within an epithelial stem cell niche. *Cell* 118(5):635-648.
27. Morris RJ*, et al.* (2004) Capturing and profiling adult hair follicle stem cells. *Nat Biotechnol* 22(4):411-417.
28. Braun KM*, et al.* (2003) Manipulation of stem cell proliferation and lineage commitment: visualisation of label-retaining cells in wholemounts of mouse epidermis. *Development* 130(21):5241-5255.
29. Jacobs JJ, Kieboom K, Marino S, DePinho RA, & van Lohuizen M (1999) The oncogene and Polycomb-group gene bmi-1 regulates cell proliferation and senescence through the ink4a locus. *Nature* 397(6715):164-168.
30. Janzen V*, et al.* (2006) Stem-cell ageing modified by the cyclin-dependent kinase inhibitor p16INK4a. *Nature* 443(7110):421-426.
31. Krishnamurthy J*, et al.* (2006) p16INK4a induces an age-dependent decline in islet regenerative potential. *Nature* 443(7110):453-457.
32. Molofsky AV*, et al.* (2006) Increasing p16INK4a expression decreases forebrain progenitors and neurogenesis during ageing. *Nature* 443(7110):448-452.
33. Signer RA, Montecino-Rodriguez E, Witte ON, & Dorshkind K (2008) Aging and cancer resistance in lymphoid progenitors are linked processes conferred by p16Ink4a and Arf. *Genes Dev* 22(22):3115-3120.
34. Su X*, et al.* (2009) Rescue of key features of the p63-null epithelial phenotype by inactivation of Ink4a and Arf. *EMBO J* 28(13):1904-1915.
35. Martinez P*, et al.* (2009) Increased telomere fragility and fusions resulting from TRF1 deficiency lead to degenerative pathologies and increased cancer in mice. *Genes Dev* 23(17):2060-2075.
36. Flores I & Blasco MA (2009) A p53-dependent response limits epidermal stem cell functionality and organismal size in mice with short telomeres. *PLoS One* 4(3):e4934.
37. Su X*, et al.* (2009) TAp63 prevents premature aging by promoting adult stem cell maintenance. *Cell Stem Cell* 5(1):64-75.
38. Akala OO*, et al.* (2008) Long-term haematopoietic reconstitution by Trp53-/-p16Ink4a-/-p19Arf-/- multipotent progenitors. *Nature* 453(7192):228-232.
39. Armesilla-Diaz A*, et al.* (2009) p53 regulates the self-renewal and differentiation of neural precursors. *Neuroscience* 158(4):1378-1389.
40. Cicalese A*, et al.* (2009) The tumor suppressor p53 regulates polarity of self-renewing divisions in mammary stem cells. *Cell* 138(6):1083-1095.
41. Clayton E*, et al.* (2007) A single type of progenitor cell maintains normal epidermis. *Nature* 446(7132):185-189.
42. Lechler T & Fuchs E (2005) Asymmetric cell divisions promote stratification and differentiation of mammalian skin. *Nature* 437(7056):275-280.
43. Serrano M*, et al.* (1996) Role of the INK4a locus in tumor suppression and cell mortality. *Cell.* 85(1):27-37.
44. Barrandon Y, Li V, & Green H (1988) New techniques for the grafting of cultured

human epidermal cells onto athymic animals. *J Invest Dermatol* 91(4):315-318.
45. Bitoun E*, et al.* (2003) LEKTI proteolytic processing in human primary keratinocytes, tissue distribution and defective expression in Netherton syndrome. *Hum Mol Genet* 12(19):2417-2430.

Figure legends:

Figure 1. *E4F1* inactivation triggers transient hyperplasia of the epidermis followed by permanent loss of epidermal cells and severe skin ulcerations. (A) Immunohistochemical (IHC) analysis of E4F1 expression in human skin or murine back skin and hair follicle (HF). Scale bar = 40µm. The dotted line indicates the dermis-epidermis junction. d: dermis. (B) Macroscopic alterations of back skin of adult *E4F1*$^{-/flox}$*; RERT* mice 7 (early) or 15 days (late) after Cre-mediated *E4F1* inactivation. (C) Representative picture of *E4F1*^{flox}*; RERT* tails at late time points (6 weeks) after 4OHT applications. (D) Hematoxylin and eosin (H/E) staining (upper panels) and Ki67 IHC analysis (lower panels) of dorsal skin sections prepared from 4OHT-treated *E4F1*$^{-/flox}$*; RERT* adult mice at early and late time points. Left panels show similar analyses performed on 4OHT-treated *E4F1*$^{+/flox}$*; RERT* control animals. Scale bar = 20µm. (E) IHC analysis of dorsal skin sections from *E4F1*$^{+/flox}$ and *E4F1*$^{-/flox}$*; K5-Cre* neonates using anti-E4F1 antibody. Scale bar = 40µm. (G) Photograph of representative *E4F1*$^{+/flox}$ and *E4F1*$^{-/flox}$*; K5-Cre* neonates (P4) showing acute symptoms of dehydration. (F) H/E staining (upper panels) and Ki67 IHC analysis (lower panels) of dorsal skin sections prepared from *E4F1*^{flox}; *K5-Cre* P4 neonates. Scale bar = 20µm. (G) Back skin from *E4F1*$^{+/flox}$*; K5* or *E4F1*$^{-/flox}$*; K5* P1 neonates engrafted onto recipient nude mice. Photographs of representative engrafted skin, 2 weeks after engrafment and H/E stained sections. Scale bar = 40µm.

Figure 2. *E4F1* inactivation results in expansion of the basal cells compartment of the epidermis and in abnormal keratinocyte differentiation *in vivo.* (A) *E4F1* inactivation results in hyperproliferation of keratin14- and α6-integrin-positive basal/TAC cells. Immunostainings of dorsal skin sections from *E4F1*$^{+/flox}$ and *E4F1*$^{-/flox}$*; K5-Cre* neonates with

anti-keratin 14 (K14) and anti-α6 integrin (α6) antibodies. (B) Immunohistochemical analysis of dorsal skin sections from *E4F1*$^{+/flox}$ and *E4F1*$^{-/flox}$*; K5-Cre* neonates with anti-Keratin6 (K6), anti-Keratin10 (K10) or anti-involucrin (invol) antibodies. Scale bar = 40µm.

Figure 3. *E4F1* inactivation results in epidermal stem cells exhaustion *in vivo* and *ex vivo*. (A) Clonogenic assays performed with primary murine keratinocytes prepared from back skin of *E4F1*^{flox}*; RERT* adult mice 6 days after 4OHT applications (*in vivo*), or from *E4F1*^{flox}*; RERT* neonatal skins and treated with 4OHT in culture medium, 24 hours after plating (*ex vivo*). Assays were also performed with primary keratinocytes isolated from *E4F1*^{flox}*; K5-Cre* neonates (P1). Rhodamine B staining was performed after 15 days of culture. Data shown are representative of experiments performed in duplicates and repeated at least 3 times. Scale bar = 1cm. (B) Clonogenic assays (left panel) performed with human primary keratinocytes transduced with retroviral vectors expressing shRNAs targeting either human E4F1 (shE4F1) or non relevant sequence (shCtrl). Quantification (right panel) of total number and size (diameter, in mm) of clones from 3 independent experiments. (C) Multiparameter FACScan analyses of primary keratinocytes isolated from *E4F1*^{flox}*; K5-Cre* P3 neonates after α6-integrin and CD34 immunostainings. The percentage of α6^{high}/CD34^{+} epidermal stem cells is indicated (Average of 3 independent experiments +/-SD). (D) Immunohistochemical analyses of back skin sections from *E4F1*^{flox}*; RERT* adult mice, 3 weeks after 4OHT applications with antibodies directed against the stem/bulge specific markers CD34 (upper panels) and keratin-15 (K15, lower panels). Arrows indicate K15- or CD34-positive stem cells located in the bulge region of hair follicles. Scale bar = 80µm. (E) Whole mounts of tail epidermis prepared from *E4F1*^{flox}*; RERT; Keratin15-GFP* mice 4 weeks after 4OHT applications. White arrows point K15-GFP^{+} ESC that locate in the bulge region of HF in control animals (*E4F1*$^{+/flox}$) treated with 4OHT (left panels). DAPI staining was

performed to show HF morphology. Scale bar = 80 µm. (F) Analyses of Long term BrdU-Retaining Cells (LRC) in whole mounts of tail epidermis prepared from *E4F1^{flox}; RERT* 16-week old mice at different time points after 4OHT applications. Anti-BrdU (green) and anti-Ki67 (Red) immunostainings of control and *E4F1 $^{-/flox}$; RERT* HF 3 (early) or 6 (late) weeks after E4F1 inactivation showing transient hyperproliferation followed by loss of LRC (white arrows). LRC locate in the bulge region of HF from control skin treated with 4OHT for 6 weeks (*E4F1$^{+/flox}$*, left panels). Scale bar = 80µm.

Figure 4. Deletion of the *Ink4a/Arf* locus partially rescues *E4F1* KO skin defects *in vivo* and *ex vivo*. (A) Quantitative analyses of *Ink4a* and *Arf* mRNA levels in *E4F1*^{flox}*; K5-Cre* freshly isolated primary keratinocytes. (B) Clonogenic assays performed with *E4F1*^{flox}*; RERT; Ink4a/Arf*$^{-/-}$ or *E4F1*^{flox}*; RERT; Ink4a/Arf*$^{+/+}$ primary keratinocytes in presence of 4OHT. One representative experiment of 3 independent experiments performed in duplicates. Quantitative analyses of the number and size (diameter, in mm) of clones was performed after 15 days in culture. (C) High magnification photograph of representative clones. Scale bar = 0,5 mm. (D) H&E stainings of dorsal skin sections prepared from 4OHT-treated *E4F1*^{flox}*; RERT; Ink4a/Arf*$^{+/+}$ 12-week old mice (upper panels) or *E4F1*^{flox}*; RERT; Ink4a/Arf*$^{-/-}$ mice (lower panels). The early epidermal hyperplasia of 4OHT-treated *E4F1$^{-/flox}$; RERT; INK4a/ARF$^{-/-}$* animals was reproducibly less severe and delayed compared to animals lacking *E4F1* only (*E4F1$^{-/flox}$; RERT; INK4a/ARF$^{+/+}$*).

Figure 5. Down-regulation of the Bmi1-Arf-p53 axis rescues *E4F1* KO ESC defects. (A) Primary keratinocytes isolated from *E4F1^{flox}; RERT* neonates were transduced with control (pMSCV) or Bmi1 encoding retroviruses (Bmi1) and used for clonogenic assays in presence of 4OHT. (B) Clonogenic assays performed with *E4F1*^{flox}*; RERT* primary keratinocytes

transduced with control (shCtrl) or p53 (shp53) shRNAs encoding lentiviruses in presence of 4OHT. In A-B, photographs (upper panels) and quantifications (lower panels) of one representative experiment. 3 independent experiments were performed in duplicates. Quantitative analyses of the number and size (diameter, in mm) of clones were performed after 10 days. (C) Western blot analyses showing ectopic overexpression of Bmi1 (left panels) in rescued *E4F1 KO* clones, or efficient shRNA-mediated depletion of p53 (center panels) in rescued *E4F1 KO* clones (right panels).

Fig1 Lacroix et al

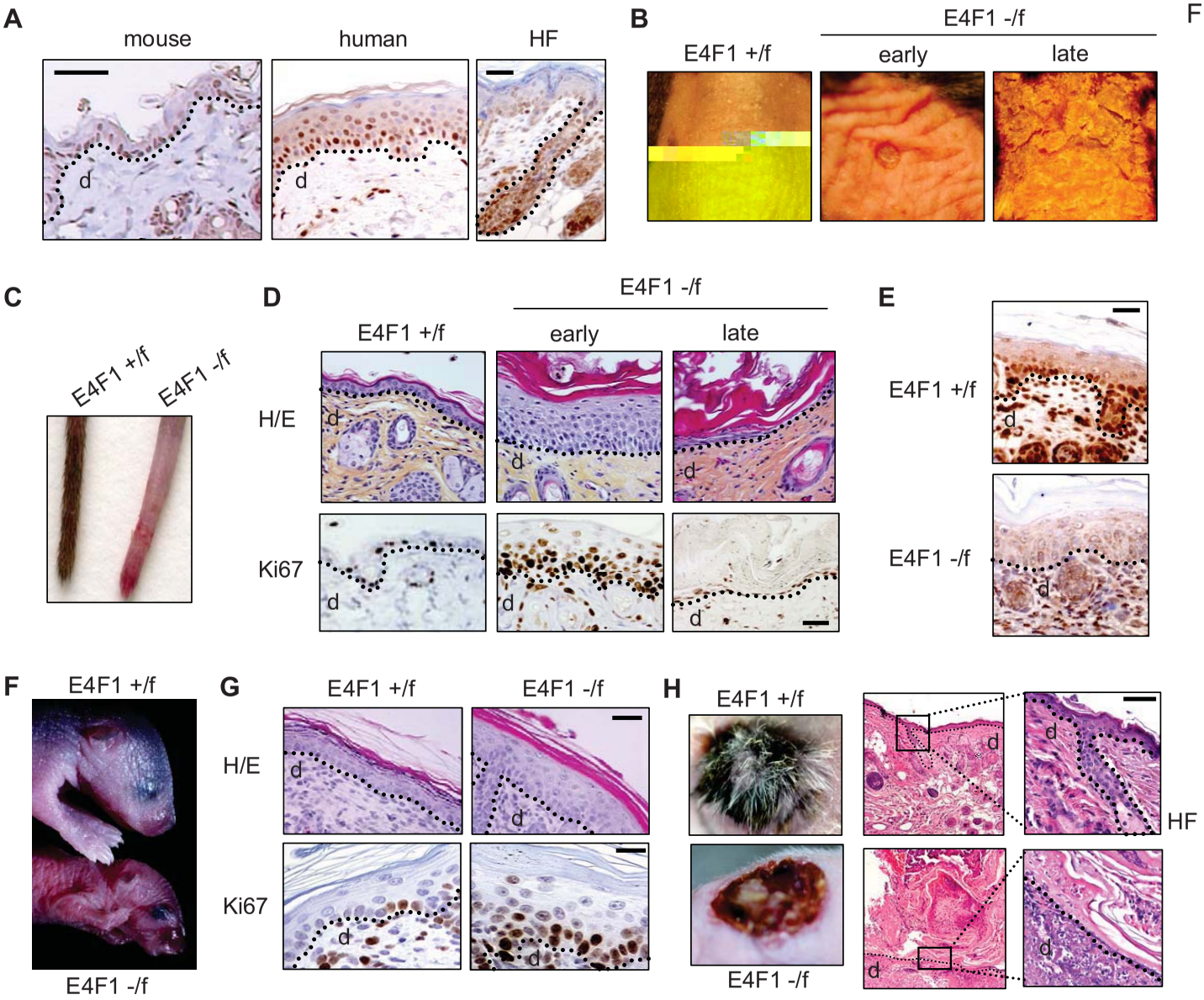

Fig2 Lacroix et al

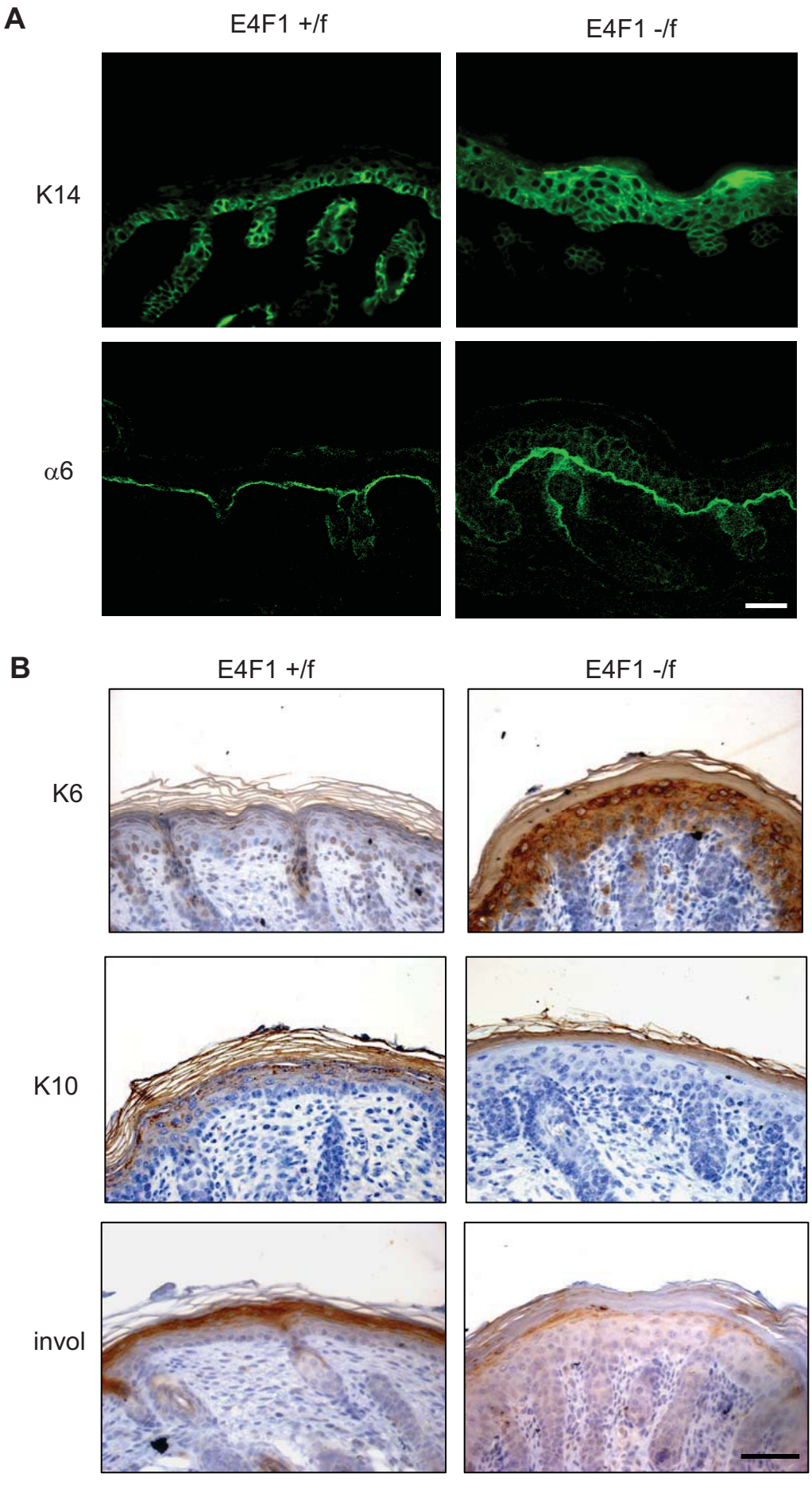

Fig3 Lacroix et al

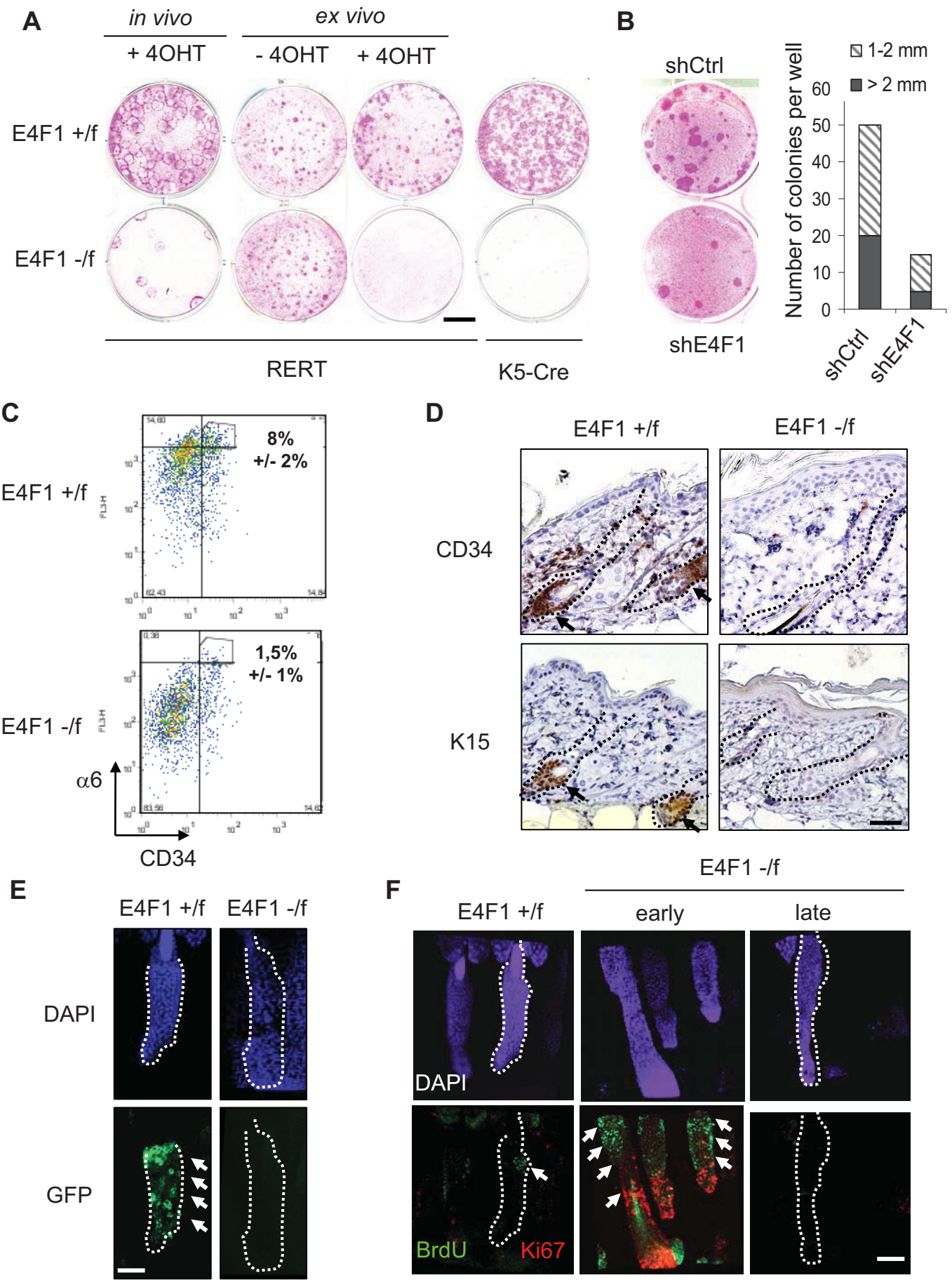

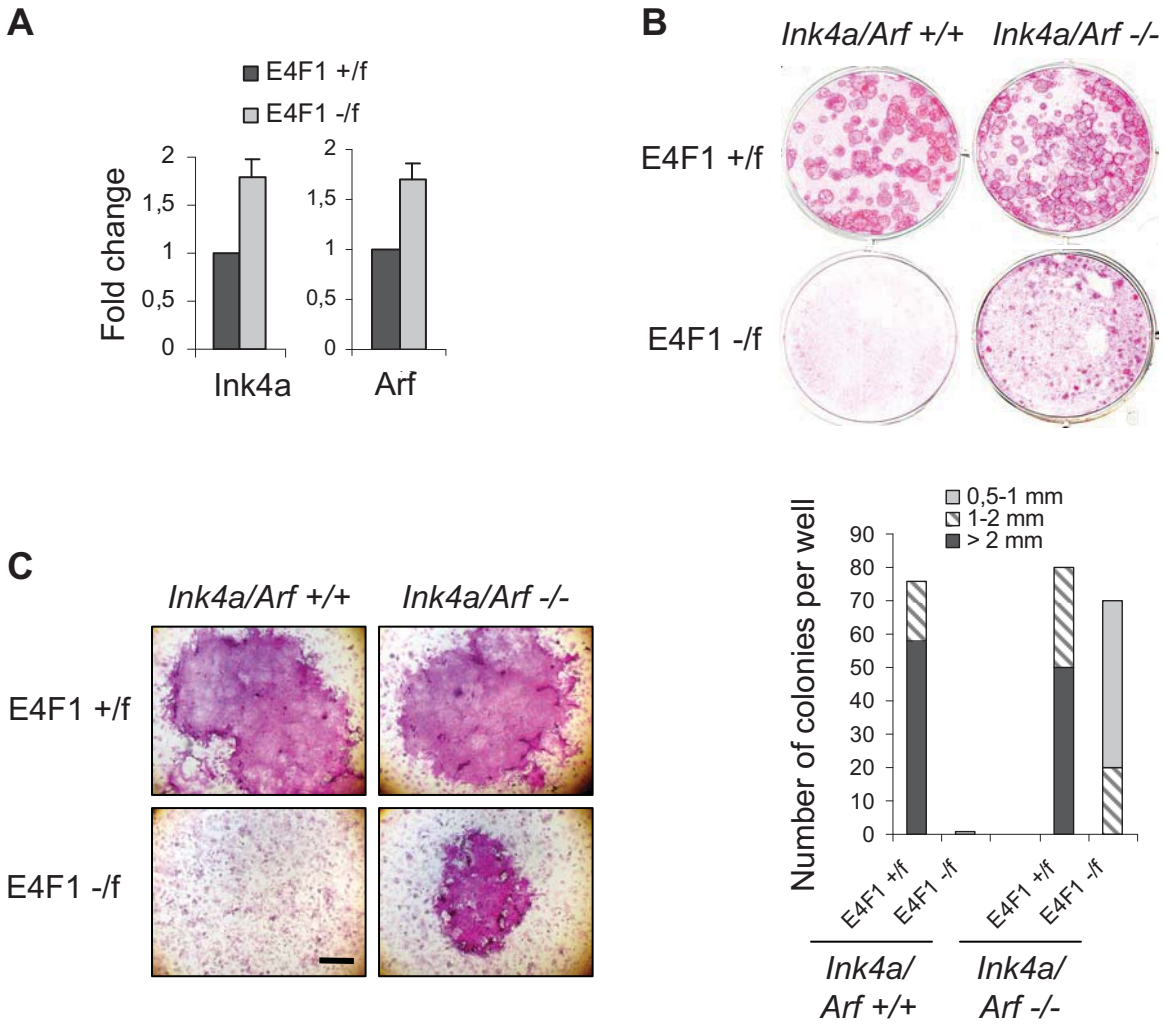
A
E4F1 +/f
E4F1 -/f
Fold change
2
1,5
1
0,5
0
Ink4a
Arf
B
Ink4a/Arf +/+
Ink4a/Arf -/-
E4F1 +/f
E4F1 -/f
C
Ink4a/Arf +/+
Ink4a/Arf -/-
E4F1 +/f
E4F1 -/f
0,5-1 mm
1-2 mm
> 2 mm
Number of colonies per well
90
80
70
60
50
40
30
20
10
0
E4F1 +/f
E4F1 -/f
E4F1 +/f
E4F1 -/f
Ink4a/ Arf +/+
Ink4a/ Arf -/-
D
E4F1 -/f
E4F1 +/f
early
late
Ink4a/Arf +/+
Ink4a/Arf -/-

Fig5 Lacroix et al

A

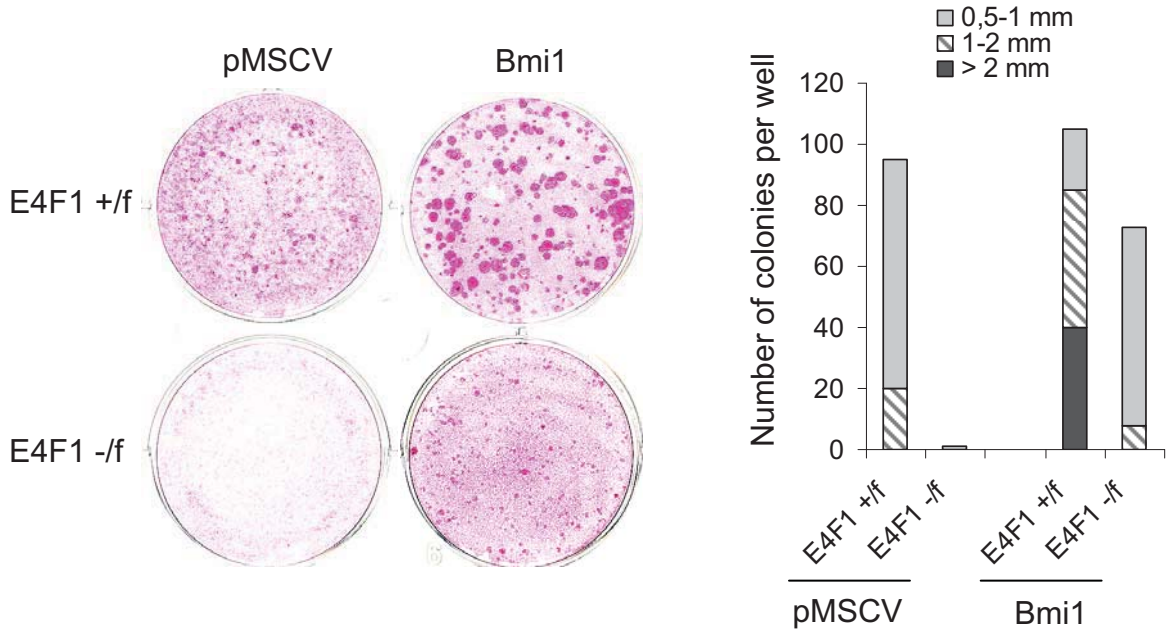

B

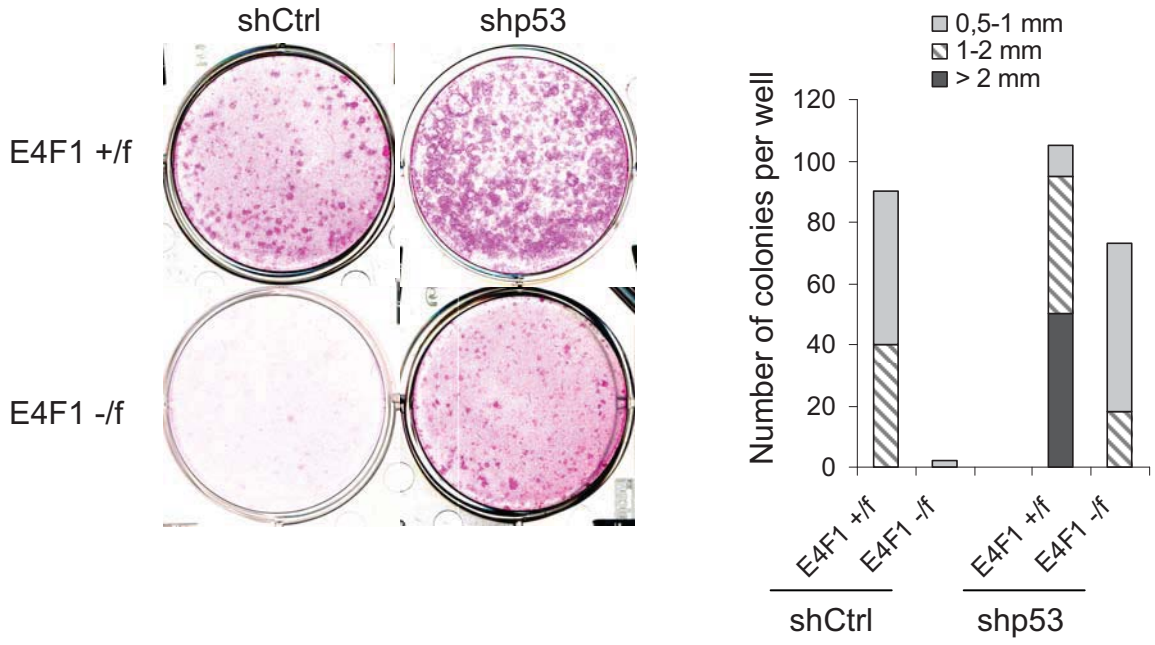

C

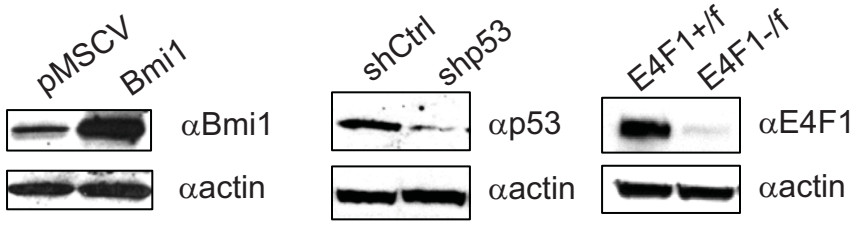

Supplementary informations: ***Lacroix M, Caramel J et al.***

Supplementary Materials & methods

Generation of *E4F1*$^{-/flox}$ mice

The E4F1 targeting construct was generated by cloning *129/SvJ* murine genomic *E4F1* sequences (11) into the pDT915 targeting vector. Lox-P sites were introduced before exon 4 and after exon 14 as indicated in supplemental figure S1. A hygromycin-TK cassette flanked by two FRT sequences was also added after the polyA signal of the *E4F1* gene. The targeting vector was linearized by NotI and electroporated in J1 ES cells (*129/SvJ*). The later were selected with hygromycin B (130µg/ml, Calbiochem) for a week before clonal amplification. Correct targeting of the *E4F1* locus was assessed on genomic DNA prepared from hygromycin-resistant ES clones by southern blotting using probes corresponding to 5' (400bp) and 3' (360bp) flanking sequences of the E4F1 gene (Figure S1). Targeted ES cells were electroporated with a Flipase expressing vector (gift of Dr. Dymecki S.) and selected using Ganciclovir (4µM) to enrich for clones in which the hygromycin-TK cassette was deleted. Several *E4F1*$^{+/flox}$ ES clones displaying a normal karyotype, were subsequently injected into *C57Bl/6* blastocysts. Chimeric mice were mated with *C57Bl/6* mice for germline transmission of the E4F1 flox allele. Heterozygous mutant mice *E4F1*$^{+/flox}$ and *E4F1*$^{+/-}$ were interbred to generate *E4F1*$^{-/flox}$ animals. *E4F1* recombination was assessed by immunoblotting or by quantitative PCR analysis on skin genomic DNA using primers specific for the *E4F1* locus, as described in Supplemental Fig. S1C-E (primer A: 5'-GGCTGCTGCGTGGATTTC, B: 5'-GCTAGGTAGGGTAGGAGGCTGTCT, C: 5'-ACCGGCGTGTTCACTCAGAC, D: 5'-GCAGAACTGGCACACGTGG, E: 5'-TTCGGTATAGTGTTGAGG, F: 5'-AGGGGCTGGGCTACAATGG).

Genotyping

E4F1^{flox}*; RERT* mice were genotyped by PCR on tail genomic DNA using the following primers: i) E4F1 wild type (*E4F1*$^{+}$) and conditional knock-out Flox alleles (*E4F1*^{flox}): 5'-CCTTGAGCACGGAGGAGAGC-3' and 5'-GCCCTAGCCTGCTC-TGCCATC-3'. ii) *E4F1* constitutive knock-out allele (*E4F1*$^{-}$): 5'-CACTGCCTTGGAGGACTTTG-3' and 5'-CCTCTGTTCCACA-TACACTTCATTC-3'. iii) wild type and knock-in *RERT* alleles: 5'-GTCAGTACACATACAGACTT-3', 5'-TGAGCGAACAGGGCGAA-3' and 5'-TCCATGGAGCACCCAGTGAA-3'. iv) *keratin5-C*re transgene: 5'-AACATGCTTCATCGTCGG-3' and 5'-TTCGGATCATCAGCTACACC-3'. v) *keratin15-GFP* transgene: 5'-CTACGGCGTGCAGTGCTTCAGC-3' and 5'-GGCGAGCTGCACGCTGCGTCCTC-3'. vi) *Ink4a/Arf* alleles: wild type 5'-ATGATGATGGGCAACGTTC-3' and 5'-CAAATATCGCACGATGTC-3'; knock-out: 5'-CTATCAGGACATAGCGTTGG-3' and 5'-AGTGAGAGTTTGGGGACAGAG-3'.

Histochemistry, immunolabelling of skin sections and whole mounts

Skin biopsies were either fixed in 4% neutral-buffered formalin (24h) and paraffin embedded, or frozen in Tissue-Tek OCT (Sakura) for cryosections. Paraffin-embedded tissues were sectioned and processed for immunohistochemistry (IHC) or hematoxylin and eosin (H/E) stainings. IHC was performed on 4μm sections using appropriate primary antibodies and the corresponding biotinylated secondary antibody coupled to streptavidin-peroxidase complex (ABC Vectastain kit, Vector Laboratories). Revelation was performed using the peroxidase substrate DAB (Vector Laboratories). All secondary antibodies were diluted at 1/200 for immunohistochemistry (DAKO) and 1/1000 for immunohistofluorescence (Alexa-Invitrogen). Apoptotic cells were detected using TUNEL staining kits (Roche) or by IHC with anti-caspase 3 antibody.

Culture of primary keratinocytes and clonogenic assays

For cell cycle analyses, BrdU (10 mM, Sigma) was added in the culture medium for 24 hours. For clonogenic assays, 2000-10000 total primary keratinocytes per well were plated on a confluent feeder layer of inactivated J2-3T3 fibroblasts (3 hour-treatment with mitomycin C at 4µg/ml, Sigma) grown on collagen-I-coated 6-well plates, at 32°C, 8% CO2 (mouse keratinocytes) or at 37°C, 10% CO2 (human keratinocytes). Clonogenic assays were performed in calcium-free DMEM-HamF12 (3:1) (Invitrogen), containing 10% calcium-free FCS (Sigma), 4mM L-Glutamine, 110mg/l Na Pyruvate, 8 ng/ml Choleratoxine, 0.4 µg/ml Hydrocortisone, 5 µg/ml Insulin (Sigma), 10 µg/ml murine EGF.

Retroviral and lentiviral particles productions and infections

Retroviral and lentiviral particles were produced in 293T cells by transient transfection using Jet-PEI reagent (Ozyme) of gag/pol, env-VSV-G, and indicated viral constructs. 48 hrs after transfection, viral supernatants were harvested and added on primary keratinocytes overnight with polybrene at 8µg/ml (Sigma). Antibiotic selection of transduced primary murine keratinocytes was performed 48 hours later with puromycin (1,25 µg/mL, pLKO1), or blasticidin (5µg/mL, pMSCV).

Legends of Supplementary figures.

Figure S1. Generation and validation of *E4F1* conditional knock-out mice. (A) Schematic representation of the unmodified (upper), the targeting vector (middle), and recombined *E4F1 flox* allele (lower). (B) Homologous recombination was verified on both ends by southern blotting using 5' (left panel) and 3' (right panel) external probes. (C) The hygromycin-thymidine Kinase (*Hygro-TK*) resistance cassette was removed *in vitro* after a second round of electroporation of homologous recombinant ES clones using the Flpe recombinase (upper panel). Schematic representation of the floxed E4F1 allele after Cre-mediated recombination (lower panel). (D) Cre-mediated recombination of the $E4F1^{flox}$ allele in skin. Quantitative (left panel) or semi-quantitative (right panel) PCR analyses were performed on genomic DNA extracted from back skin of $E4F1^{+/-}$ or $E4F1^{-/flox}$; *RERT* adult mice after topical application of 4OHT, or from back skin of $E4F1^{+/-}$ or $E4F1^{-/flox}$; *K5-Cre* P1 neonates. The primer pairs used for PCR amplifications are indicated by arrows in (C). Note that primers pair A/B generates a PCR amplicon only after Cre-mediated recombination. Normalisation for equal amount of genomic DNA in those assays was controlled with primers (E/F) located in the non-recombined region of the *E4F1* locus. (E) Immunoblots showing E4F1 expression after Cre-mediated recombination in primary keratinocytes isolated from $E4F1^{flox}$; *RERT*, and treated with 4OHT, or from $E4F1^{flox}$; *K5* neonatal epidermis (right panel). ns: non-specific signal.

Figure S2. *E4F1* inactivation results in hyperproliferation of epidermal cells. Immunofluorescent images of dorsal skin sections prepared from 4OHT-treated $E4F1^{flox}$; *RERT* adult mice injected with BrdU (4h), immunostained with anti-BrdU (red) antibody and co-stained with DAPI (blue). The dashed line indicates the basal membrane and interface between epidermis (top) and dermis (bottom). Scale bar = 50 µm. Genotype of the analysed mice is indicated. Histogram shows the quantification of the percentage of BrdU-positive

cells in a representative experiment.

Figure S3. *E4F1* inactivation results in skin autonomous effects in the RERT model. Back skin from *E4F1*$^{+/flox}$*; RERT* or *E4F1*$^{-/flox}$*; RERT* P1 neonates was engrafted onto recipient nude mice and treated with 4OHT. Photographs at low (left panels) or higher (middle panels) magnification of representative engrafted skin, 2 weeks after *E4F1* inactivation. H/E stained sections of engrafted skins showing hyperplasia of E4F1 depleted epidermis (right panels). Scale bar = 40µm.

Figure S4. *E4F1* inactivation results in expansion of the basal cells compartment of the epidermis and in abnormal keratinocyte differentiation. (A) *E4F1* inactivation results in hyperproliferation of keratin14- and α6-integrin-positive basal/TAC cells. Immunostainings of dorsal skin cryosections from *E4F1*$^{+/flox}$ and *E4F1*$^{-/flox}$*; RERT* mice with anti-keratin 14 (K14) and anti-α6 integrin (α6) antibodies. Scale bar = 40µm. (B) Immunohistochemical analysis of dorsal skin sections from *E4F1*$^{+/flox}$ and *E4F1*$^{-/flox}$*; RERT* mice with anti-Keratin6 (K6), anti-Keratin10 (K10) or anti-involucrin (invol) antibodies. Scale bar = 40µm.

Figure S5. *E4F1* inactivation does not enhance the short term proliferation of primary keratinocytes in culture. (A) *E4F1* inactivation *in vitro* does not result in murine keratinocyte hyperproliferation. Cell cycle profiles of murine *E4F1*$^{+/flox}$ or *E4F1*$^{-/flox}$*; RERT* primary keratinocytes after 5 days of culture in presence of 4OHT. The percentage of cells in each phase of the cell cycle was determined by FACS scan analyses after Propidium Iodide (PI)/BrdU co-staining. (B) *E4F1*-depletion *in vitro* does not result in human keratinocyte hyperproliferation. PI/BrdU co-staining profiles of human primary keratinocytes transduced with retroviral vectors expressing either a shRNA targeting human E4F1 (shE4F1) or a

control shRNA (shCtrl). Western blot analysis (right panels) of total protein extracts showing efficient E4F1 depletion. (C) Anti-Phospho Histone H3 / PI labelling and FACScan analyses of murine *E4F1*$^{+/flox}$ or *E4F1*$^{-/flox}$*; RERT* primary keratinocytes after 5 days of culture in presence of 4OHT. Nocodazole treated cells (Noco, 10µM) were used as positive control. (D) Immunohistochemical analysis of dorsal skin sections from *E4F1*$^{+/flox}$ or *E4F1*$^{-/flox}$*; K5-Cre* P1 neonates with anti-Phospho Histone H3 antibody. The number of PPH3 positive cells per field is indicated.

Figure S6. *E4F1* inactivation results in loss of Keratin15 stem cell marker expression. Immunostaining of HF with anti-keratin15 (K15, red) in whole mounts of tail epidermis prepared from *E4F1*$^{-/flox}$*; RERT* and control mice 6 weeks after 4OHT applications. Small inset represents the same HFs after anti-integrinα6 (α6, green) and DAPI costaining (blue) to show general morphology. HF K15+ bulge region is indicated by a white bracket. Scale bar = 50 µm.

Figure S7. *E4F1* inactivation triggers hyperproliferation of LRC. Analysis of BrdU-labelled LRC cells (green) and of proliferative cells (Ki67, Red) in whole mounts of tail epidermis prepared from *E4F1*$^{-/flox}$*; RERT* mice 2 weeks after 4OHT applications. Lower magnification image of the same HF after DAPI staining (blue) to show general morphology. BrdU and Ki67 double positive HF LRC stem cells are indicated by white arrows. Scale bar = 50 µm.

Figure S8. E4F1 inactivation alters wound healing. A punch was made on the back skin of *E4F1*$^{+/flox}$ and *E4F1*$^{-/flox}$*; RERT* mice treated with 4OHT and its closure observed at the indicated times.

FigureS1
Lacroix et al

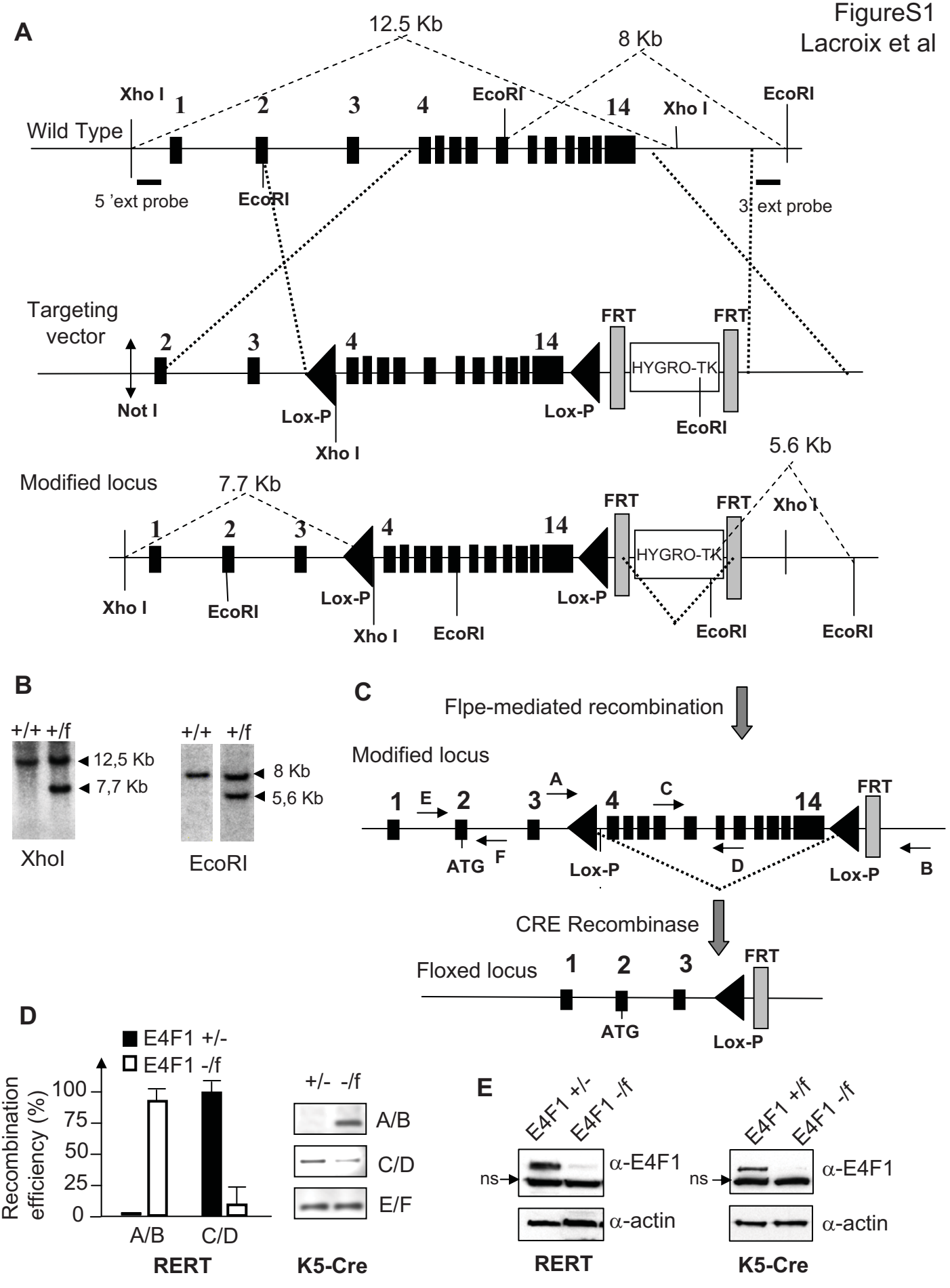

FigureS2
Lacroix et al

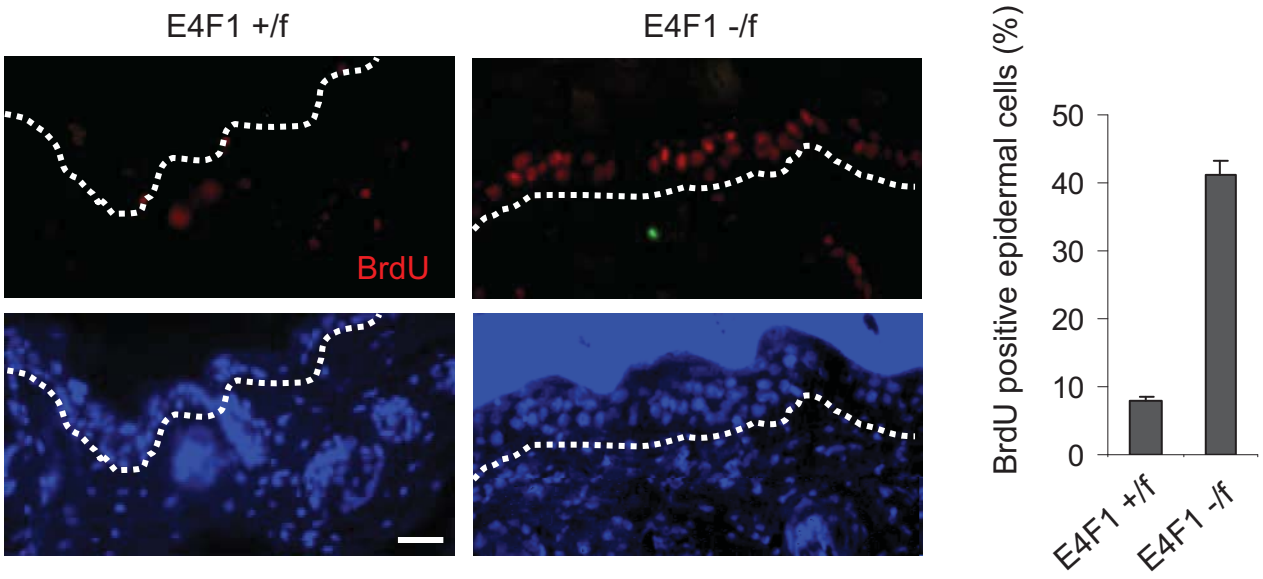

Figure S3 Lacroix et al

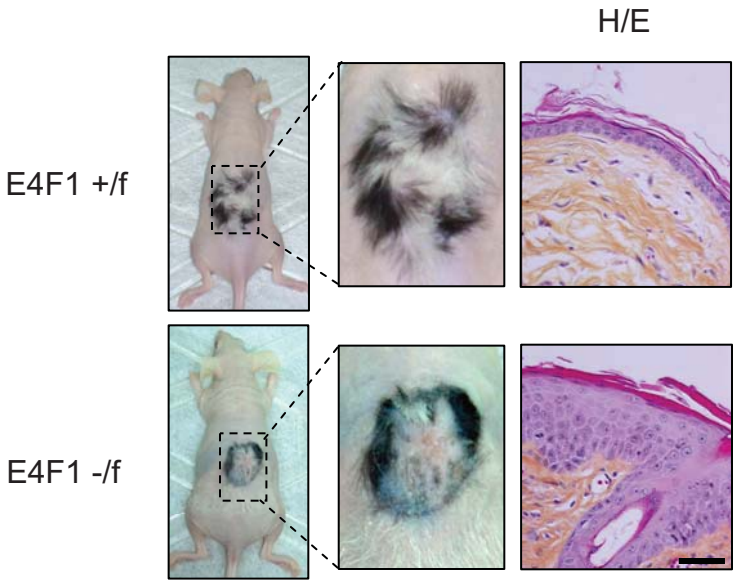

Figure S4 Lacroix et al

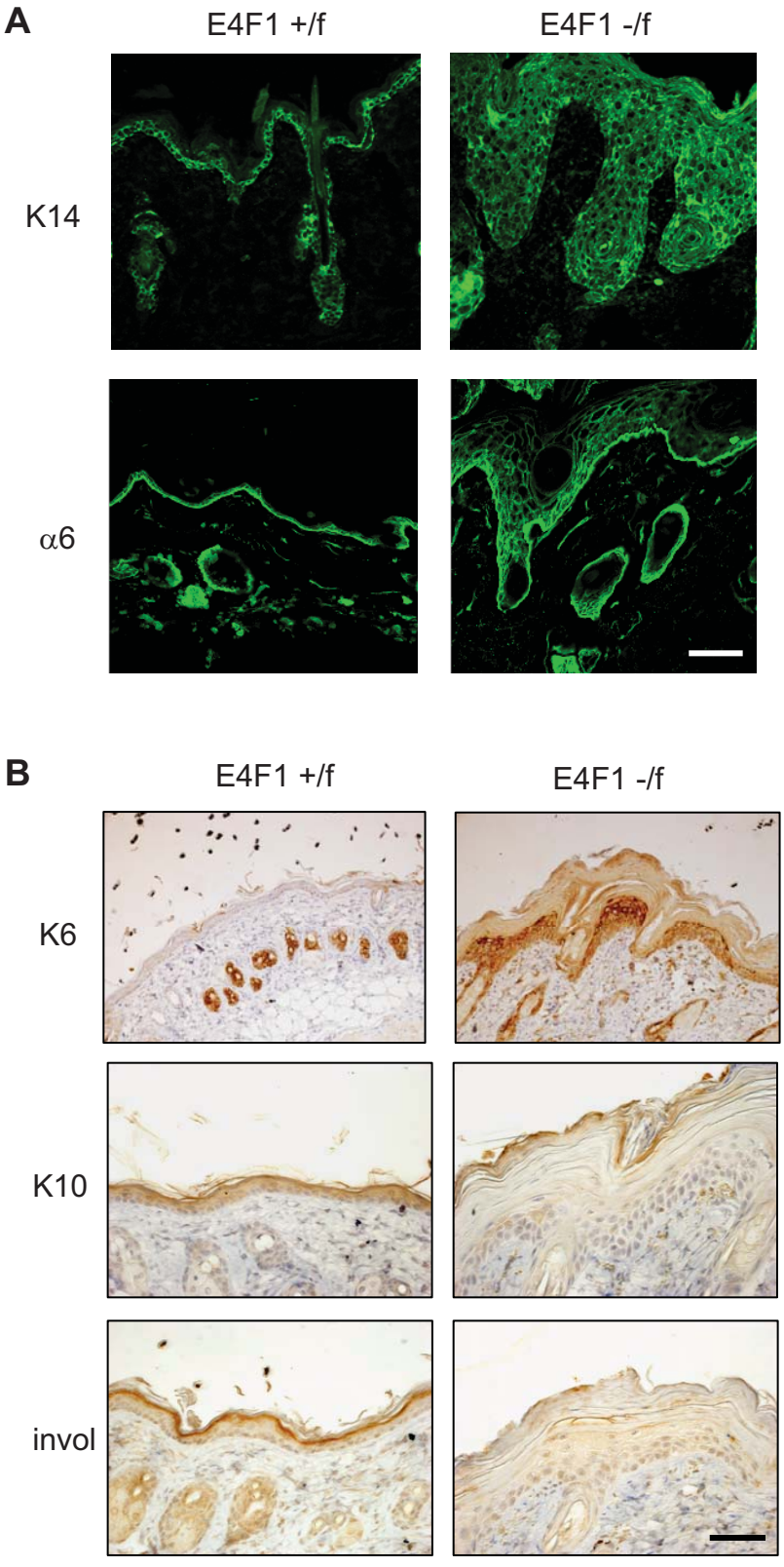

Figure S5 Lacroix et al

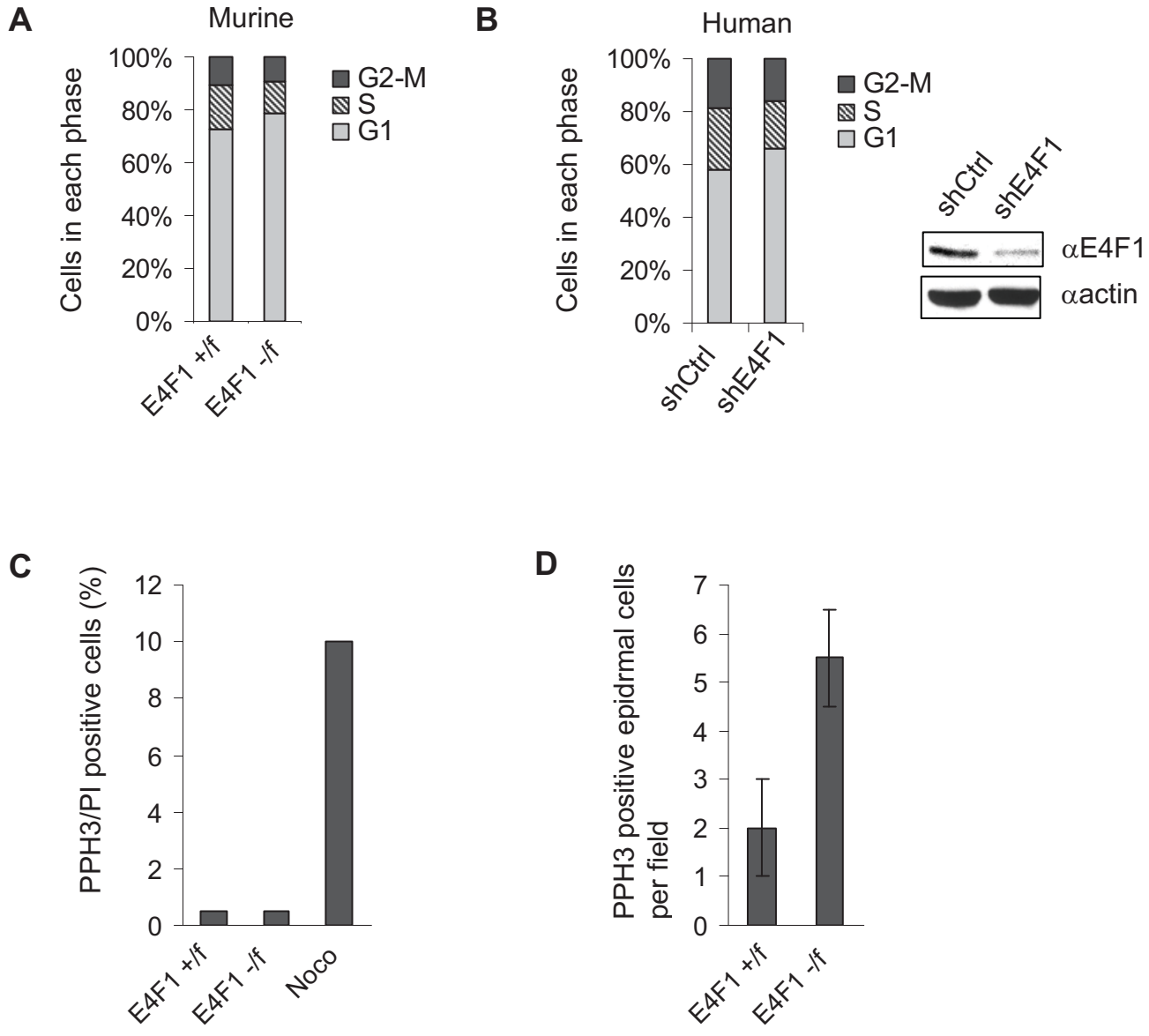

Figure S6 Lacroix et al

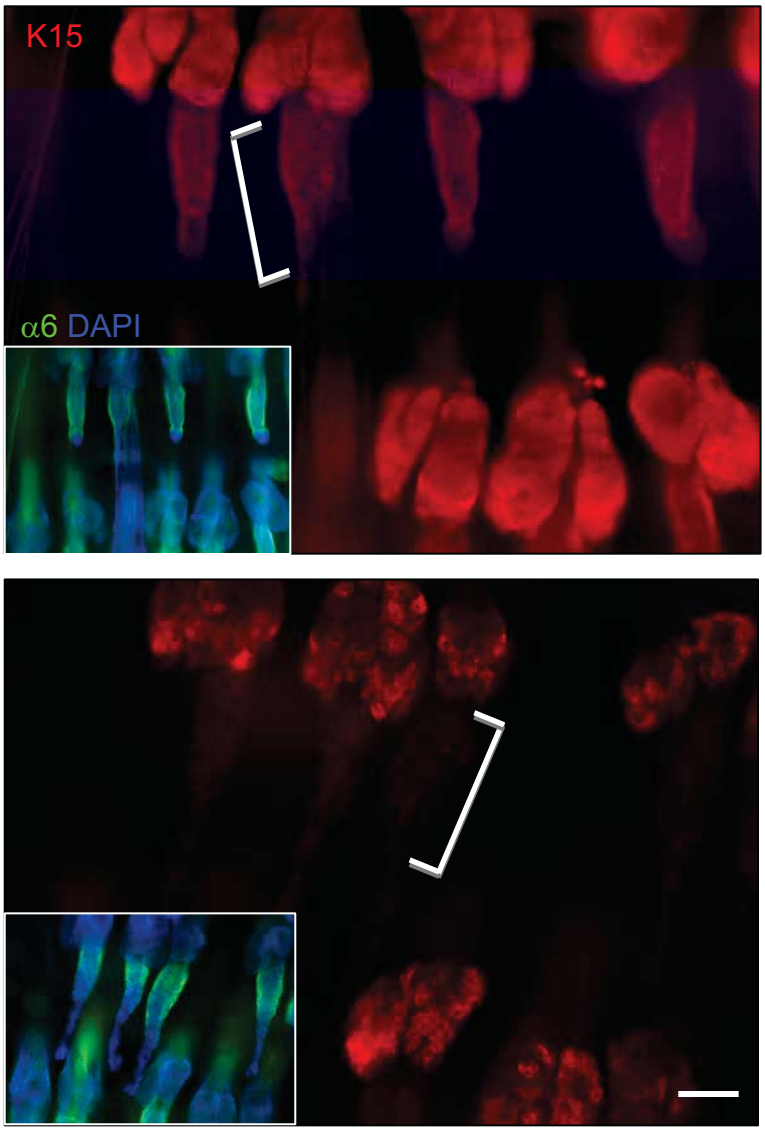

Figure S7 Lacroix et al

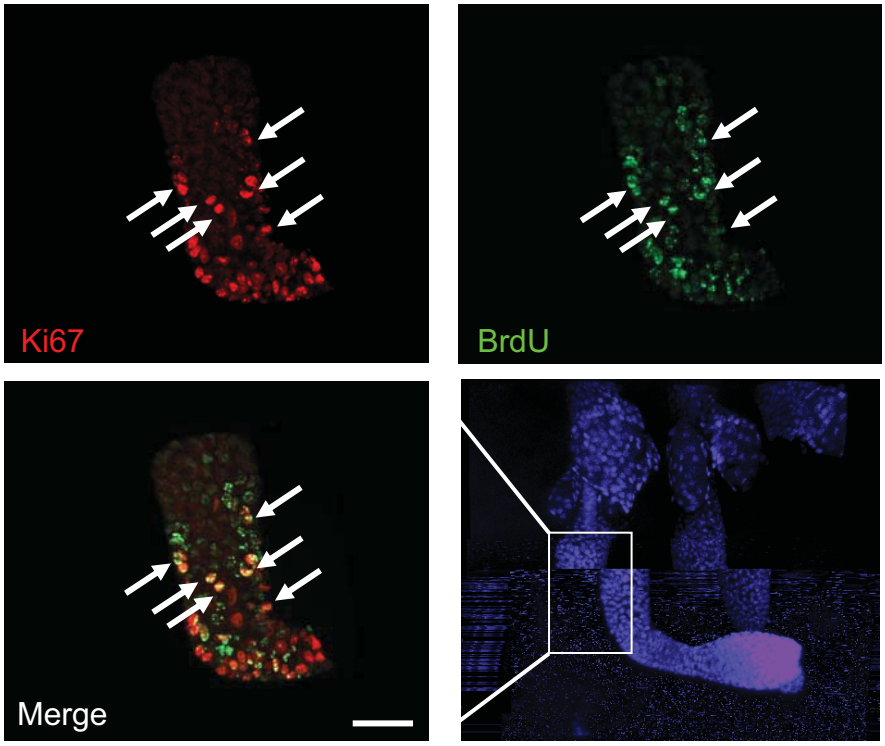

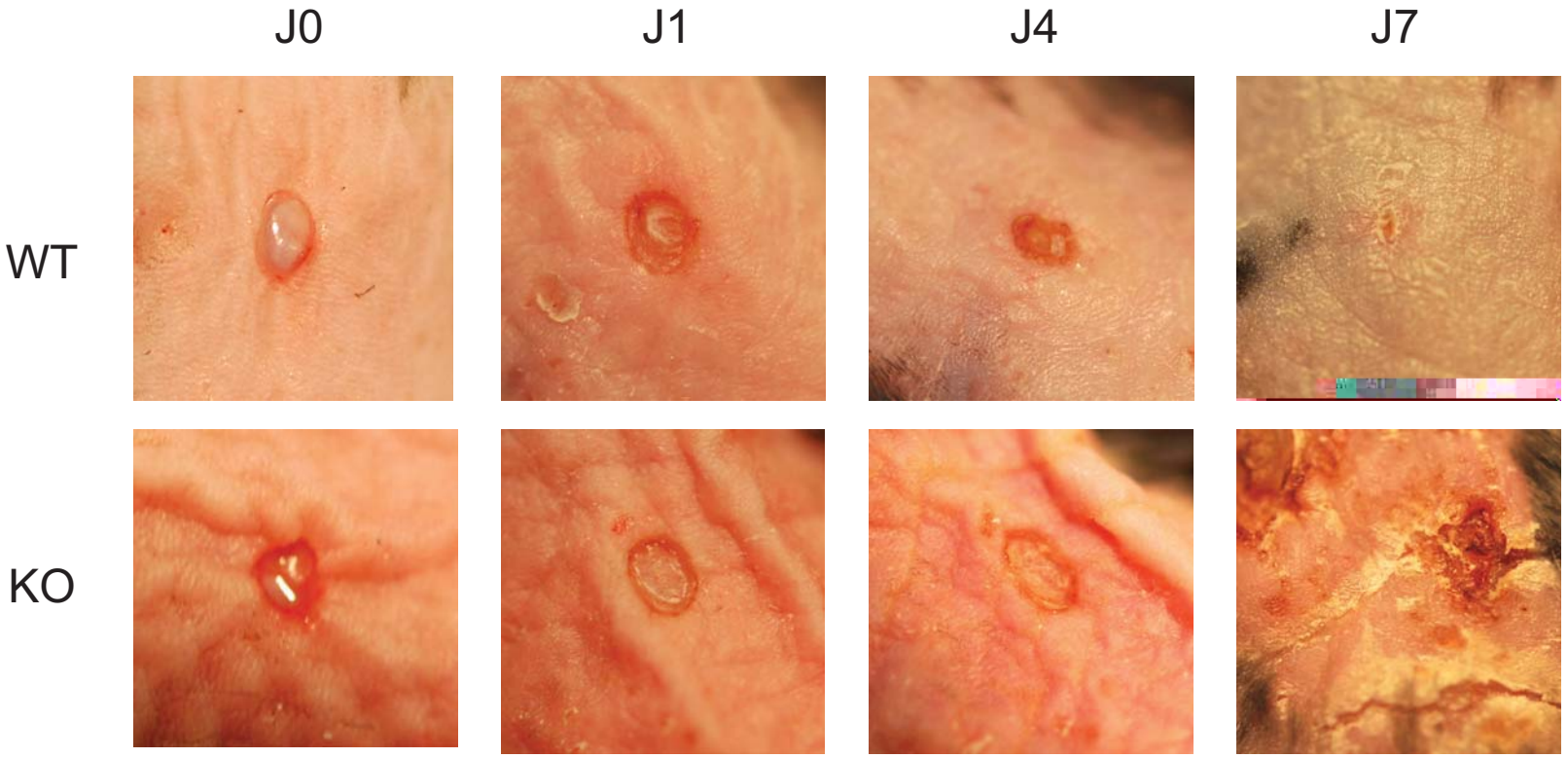
J0
J1
J4
J7
WT
KO